LSU #7011

Advanced Thin Ionization Calorimeter (ATIC) Balloon Experiment

NASA Grant NAG5-5064

(LSU Account: 115-30-5108)

Final Technical Report

Submitted to

National Aeronautics and Space Administration
Grants Office
Code 218
GSFC Wallops Flight Facility
Wallops Island, VA 23337-5009

Submitted by

Department of Physics and Astronomy
Louisiana State University
Baton Rouge, LA 70803-4001
225-578-8696

John P. Wefel, PI (wefel@phunds.phys.lsu.edu)
T. Gregory Guzik, Co-I (guzik@phunds.phys.lsu.edu)
Joachim B. Isbert, Instr. Man. (isbert@phunds.phys.lsu.edu)

The Advanced Thin Ionization Calorimeter (ATIC) Balloon Experiment NAG5-5064

Project Summary

During grant NAG5-5064, LSU led the ATIC team in the development, construction, testing, accelerator validation, pre-deployment integration and flight operations of the Advanced Thin Ionization Calorimeter (ATIC) Balloon Experiment. This involved interfacing among the ATIC collaborators (UMD, NRL/MSFC, SU, MSU, MPI, SNU) to develop a new balloon payload based upon a fully active calorimeter, a carbon target, a scintillator strip hodoscope and a pixilated silicon solid state detector for a detailed investigation of the very high energy cosmic rays to energies beyond 10^{14} eV/nucleus. It is in this very high energy region that theory predicts changes in composition and energy spectra related to the Supernova Remnant Acceleration model for cosmic rays below the "knee" in the all-particle spectrum.

This report provides a documentation list, details the anticipated ATIC science return, describes the particle detection principles on which the experiment is based, summarizes the simulation results for the system, describes the validation work at the CERN SPS accelerator and details the balloon flight configuration. The ATIC experiment had a very successful LDB flight from McMurdo, Antarctica in 12/00 – 1/01. The instrument performed well for the entire 15 days. Preliminary data analysis shows acceptable charge resolution and an all-particle power law energy deposition distribution not inconsistent with previous measurements. Detailed analysis is underway and will result in new data on the cosmic ray charge and energy spectra in the GeV-TeV energy range. ATIC is currently being refurbished in anticipation of another LDB flight in the 2002-03 period.

The Advanced Thin Ionization Calorimeter (ATIC) Balloon Experiment

Publications, Proceedings, Reports and Documents

A. Publications and Proceedings

The ATIC Experiment: First Balloon Flight, J. P.Wefel for the ATIC Collaboration, *Proc. 27th Int'l Cosmic Rays Conf. (Hamburg)*, **6**, 2111 (2001)

Preliminary Results from the First Flight of ATIC, E. S. Seo for the ATIC Collaboration, *Proc. 27th Int'l Cosmic Rays Conf. (Hamburg)*, **5**, 1601 (2001)

The First Flight of ATIC: Preliminary Results on Li, Be, B Nuclei, V. I. Zatsepin for theATIC Collaboration, *Proc. 27th Int'l Cosmic Rays Conf. (Hamburg)*, **5**, 1605 (2001)

The CNO Concentration in Cosmic Ray Spectrum as Measured from the AdvancedThin Ionization Calorimeter Experiment, A. R. Fazely and R. M. Gunasingha for the ATIC Collaboration, *Proc. 27th Int'l Cosmic Rays Conf. (Hamburg)*, **5**, 1595 (2001)

Preliminary Results from the First Flight of ATIC: Z>8 Spectra, J. H. Adams, Jr. for the ATIC Collaboration, *Proc. 27th Int'l Cosmic Rays Conf. (Hamburg)*, **5**, 1599 (2001)

High Energy Electron Detection with ATIC, J. Chang and W. K. H. Schmidt for the ATIC Collaboration, *Proc. 27th Int'l Cosmic Rays Conf. (Hamburg)*, **6**, 2115 (2001)

ATIC Flight Data Processing, H. S. Ahn for the ATIC Collaboration, *Proc. 27th Int'l Cosmic Rays Conf. (Hamburg)*, **6**, 2119 (2001)

Preliminary Results from the First Flight of ATIC: The Silicon Matrix, J. H. Adams, Jr. for the ATIC Collaboration, *Proc. 27th Int'l Cosmic Rays Conf. (Hamburg)*, **6**, 2127 (2001)

The ATIC Experiment: Performance of the Scientillator Hodoscope and the BGO Calorimeter, J. Isbert for the ATIC Collaboration, *Proc. 27th Int'l Cosmic Rays Conf. (Hamburg)*, **6**, 2123 (2001)

First Results from ATIC Beam-Test at CERN, O. Ganel, et al., the ATIC Collaboration, Adv. Space Res., (2000).

The Advanced Thin Ionization Calorimeter (ATIC) for Studies of High Energy Cosmic Rays, T. G. Guzik, J. Adams Jr., J. Ampe et al., *Proc. 26th Int'l Cosmic Rays Conf. (Salt Lake City)*, **5**, 9 (1999)

On the Detection and Identi.fication of Cosmic Gamma-Rays in a Cosmic Ray Detector, J. Chang, W. K. H. Schmidt, O. Ganel et al., *Proc. 26th Int'l Cosmic Rays Conf. (Salt Lake City)*, **5**, 37 (1999)

On the Identi.cation of High Energy Cosmic Ray Electrons in the Advanced Thin Ionization Calorimeter (ATIC), W. K. H. Schmidt, J. Chang, O. Ganel et al., *Proc. 26th Int'l Cosmic Rays Conf. (Salt Lake City)*, **5**, 41 (1999)

Silicon Matrix Detector for ATIC, J. H. Adams Jr., J. Ampe, G. Bashindzhagyan et al., *Proc.* 26th Int'l Cosmic Rays Conf. (Salt Lake City), **5**, 76 (1999)

"The CR-1 Chip: Custom VLSI Circuitry for Cosmic Rays", Adams, J.H., et al., the ATIC Collaboration, Proc 26th Int. Cosmic Ray Conf. (Salt Lake City), **5**, 69 (1999)

Data Processing and Event Reconstruction for the ATIC Balloon Payload, O. Ganel, J. H. Adams Jr., J. Chang et al., *Proc. 26th Int'l Cosmic Rays Conf. (Salt Lake City)*, **5**, 453 (1999)

Simulation of the Ion Interaction for the ATIC Experiment, H. J. Kim, S. K. Kim T. Y. Kim et al., *Proc. 26th Int'l Cosmic Rays Conf. (Salt Lake City)*, **1**, 17 (1999)

ATIC as a Tested for the ACCESS Baseline Calorimeter, J. Isbert, J. H. Adams Jr., J. Authement et al., *Space Tech. and Appl. Int'l Forum-1999*, ed. Mohamed S. El-Genk, The American Institute of Physics, **CP458**, 266 (1999)

"Improving Cosmic-ray Composition Determination Through Better Tracking", O. Ganel and E.S. Seo, the ATIC Collaboration, *Adv. Space Res.*, (1998)

Cosmic Ray Shower Simulation and Reconstruction for the ATIC Experiment, J. Z. Wang, E. S. Seo, J. H. Adams Jr. et al., *Proc. 25th Int'l Cosmic Rays Conf. (South Africa)*, **5**, 5 (1997)

Advanced Thin Ionization Calorimeter to Measure Ultrahigh Energy Cosmic Rays, E.S. Seo, et al., the ATIC Collaboration, *Adv. Space Res.*, **19**, 5, 711 (1997)

Investigations of Origin of the Primary Cosmic Rays in the International Balloon Experiment ATIC O. V. Dudnik, J. H. Adams Jr., G. L. Bashindzhagyan et al., *Proc. of the All-Ukrainian Astronomical Conf. (Kyiv)*, p. 15 (1997)

The Advanced Thin Ionization Calorimeter (ATIC) Balloon Experiment: Instrumentation, T. G. Guzik, J. H. Adams Jr., G. Bashindzhagyan et al., *Proc. The Int'l Sympos. on Optic. Sci., Eng. and Instrum. (Colorado)*, **2806**, 122 (1996)

The Advanced Thin Ionization Calorimeter (ATIC) Balloon Experiment: Expected Performance, E. S. Seo, J. H. Adams Jr., G. L. Bashindzhagyan et al., *Proc. The Int'l Sympos. on Optic. Sci., Eng. and Instrum. (Colorado)*, **2806**, 134 (1996)

Advanced Thin Ionization Calorimeter (ATIC), J. Isbert, T.G. Guzik, R. Lockwood et al., *Proc. 24th Int'l Cosmic Ray Conf.* (Rome), **3**, 718 (1995)

B. Technical Reports:

"Failure Analysis of the ATIC Kevlar Pressure Vessel for the Antarctic 2000-01 Test Flight," T.G. Guzik, Louisiana State University, LSU 00-03, 09/13/00

"ATIC Pressure Vessel Background and Test of August 26, 2000," T.G. Guzik, Louisiana State Univesity, LSU 00-02, 09/09/00

"Spill Structure for Two 375 GeV Proton Runs at CERN", T. G. Guzik, Louisiana State University, LSU 00-01, 05/10/00

"Silicon Matrix Detector for ATIC", J.H. Adams Jr. et al., Naval Research Laboratory, NRL 00-02, 05/09/00

"The Effect of Pre-trigger Timing Jitter on Charge Resolution", J. H. Adams Jr. and J. Kuznetsov, Naval Research Laboratory, NRL 00-01, 05/06/00

"RPC (Remote Procedure Call): Client API Documentation", Michael Stewart, Louisiana State University LSU 99-05, 07/21/99

"ATIC Flight Data Record Format", T.G. Guzik & B. Price, Louisiana State University, LSU 99-03, 02/15/99

"CERN Accelerator Calibration Plan", T.G. Guzik, J. Isbert, & J.P. Wefel, Louisiana State University, LSU 99-04, 01/13/99

"An Assessment of the CDF Format", T. G. Guzik, Louisiana State University, LSU 98-07 08/26/98

"Investigation of the Effects of the Post-Pulse Recovery of the ACE Chip", J.H. Adams, Jr., Naval Research Laboratory, NRL 98-5, 7/2/98

"Simulation of Protons and Alphas in the Silicon Matrix", J.H. Adams, Jr., Naval Research Laboratory, NRL 98-6, 7/13/98

"ATIC Coincidence Logic Module: Updated Logic Diagrams", T. Gregory Guzik, Louisiana State University, LSU 98-06, 5/26/98

"ATIC Coincidence Logic Module: Timing", T. Gregory Guzik, Louisiana State University, LSU 98-05, 5/26/98

"Useful Commands for QNX OS", Ram Mohan, Louisiana State University, LSU 98-04, 03/05/98

"NSBF Simulator Operator Manual", Ram Mohan, Louisiana State University, LSU 98-03, 04/05/1998

"ATIC Coincidence Logic Module: Logic & Thresholds", T. Gregory Guzik, Louisiana State University, LSU 98-01, 03/16/98

"Overview of ATIC Flight and Ground Data Systems", Brad Price, Louisiana State University, LSU 98-02, 03/12/98

"ACE for ATIC", C. Dion-Schwarz, Naval Research Laboratory, NRL 97-1 10/01/97

"ATIC Coincidence Logic Module: Interfaces", T. G. Guzik, Louisiana State University, LSU 97-10, 12/18/97

"Getting Started with CDF", Ram M. Suryanarayana & T. G. Guzik, Louisiana State University, LSU 97-11, 12/16/97

"Addition of S4 into the ATIC Experiment", Joachim Isbert, Louisiana State University, LSU 97-09, 09/10/97

"Examining Potential Data Formats for ATIC", R.M. Suryanarayana, & T.G. Guzik, Louisiana State University, LSU 97-08 07/08/97

"Calorimeter Tray Design and Readout Concept", J. Isbert & R. Lockwood, Louisiana State University, LSU 97-07, 6/27/97

"Test of 5 inch BGO crystals from S&R Rubicon/Marketech", Joachim Isbert, Louisiana State University, LSU 97-06, 06/06/97

"ATIC Scintillator Saturation and Dynamic Range", T. Gregory Guzik, Louisiana State University, LSU 97-05, 05/26/97

"Proposed DIM/ACLB Command List", C. Dion- Schwarz, Naval Research Laboratory, NRL 97-03, 04/04/97

"ATIC Coincidence Logic System: Requirements and Design", T. Gregory Guzik, Louisiana State University, LSU 97-04, 3/13/97

"NSBF Simulator Design Document", Brad Price, Louisiana State University, LSU 97-02, 3/5/97

"ATIC Baseline configuration", J. R. Lockwood, Louisiana State University, LSU 97-03, 2/26/97

C. Interface Control Documents:

Interface Control Document for the Pre Trigger Logic Board (PTLB) of the Advanced Thin Ionization Calorimeter (ATIC), J. Ampe, S.B. Ellison, J.H. Adams Jr., J.P. Wefel, Louisiana State University, #ATIC-NRL-ICD-98-04, 13 November 1998

Interface Control Document for the Front End Module (FEM) of the Advanced Thin Ionization Calorimeter (ATIC), J. Ampe, S.B. Ellison, J.H. Adams, Jr., J.P. Wefel, Louisiana State University, #ATIC-NRL-ICD-98-01, 11 September 1998

Interface Control Document for the ATIC Power System (APS) of the Advanced Thin Ionization Calorimeter (ATIC), M.A. Sen, S.B. Ellison, T. G. Guzik, J.H. Adams, Jr., J.P. Wefel, Louisiana State University, #ATIC-LSU-ICD-97-12, 13 February 1998

Interface Control Document for the Detector Interface Module (DIM) of the Advanced Thin Ionization Calorimeter (ATIC), S.B. Ellison, C. Schwarz, J. Ampe, B.W. Price, D. Wagner, T.G. Guzik, J.H. Adams, Jr., J.P. Wefel, Louisiana State University, #ATIC-LSU-ICD-97-01, 2 February 1998

Technical Discussion

A. Introduction

The Advanced Thin Ionization Calorimeter (ATIC) Balloon Experiment is designed to investigate the energy spectra of Galactic Cosmic Rays (GCR) in the high energy ($>10^{12}$ eV) regime. Cosmic rays are the only sample of matter from other regions of the galaxy which can be directly observed by experiments in the solar system. Understanding the origin and acceleration of these particles provides an important probe into the matter - energy cycle in our galaxy. ATIC addresses the high energy frontier, i.e. direct measurements to as high an energy as possible from balloon platforms. Since the cosmic rays follow a steep power law energy spectrum ($dN/dE \propto E^{-2.75}$), the high energy limit is set by exposure. Consequently, ATIC is designed for a series of Long Duration Balloon flights from, principally, McMurdo, Antarctica, or Fairbanks, AK, if this route is available.

The ATIC team has developed, built and tested the instrument, including a validation of the concept with an accelerator run at the CERN SPS. All flight systems were completed, and ATIC had a successful first ("test") flight from McMurdo, Antarctica in Dec. 00/Jan. 01. It is planned to re-fly the ATIC instrument in CY 2002.

The ATIC team is an international collaboration of researchers from the US, Russia, Korea, and Germany. The team is divided into two main functional units: hardware and simulation/modeling. The hardware development effort has been coordinated by LSU and involved the Naval Research Laboratory (NRL), Moscow State University (MSU) and Southern University (SU). The simulation/modeling effort is coordinated by the University of Maryland (UMD) and involved Seoul National University (SNU) and Max-Planck Institute-Lindau (MPI) plus some work at MSU and SU. This approach has allowed the two teams to work independently, yet, symbiotically, to produce the ATIC flight instrument and to validate its performance. For the flight phase of the ATIC project, we maintain this approximate division with the hardware team shifting to flight operations (including re-furbishment and re-building between flights) and the simulation/modeling group shifting to data processing and analysis (including additional simulations, as required). The entire collaboration is involved in the astrophysical interpretation and publication of the ATIC results.

B. Scientific Rationale

The goal of the ATIC project is to obtain new measurements of the energy spectra of individual elements in the cosmic rays, particularly H and He, over a very wide energy range (with a single instrument), from well below 10^{12} eV/particle to beyond 10^{14} eV/particle. Such data will allow us to search for spectral effects that would indicate the nature of the cosmic ray "accelerator". This work was motivated, in part, by previous experiments whose results are "tantalizing" and, in part, by theoretical developments related to particle acceleration in Supernova Remnants (SNR).

Figure B.1 shows the summary of high energy data from the NRC report "Opportunities in Cosmic-Ray Physics and Astrophysics" (Gaisser et al., 1995) as a function of magnetic rigidity for groups of indidual elements. (Here "Fe" refers to 17=Z-28.) It was expected that, if all

species come from the same sources and have the same propagation history in the galaxy, then the spectra at high energy (above ~100 GV) should have the same shape! This is clearly not the case as inspection of Figure B.1 shows, and this indicates that we have, still, much to learn about the sources, acceleration and the propagation of the GCR. We know that cosmic rays fill the galaxy and, treated as a hot gas, contribute an important "pressure" to the dynamical balance of the interstellar medium (ISM). Synchrotron emission indicates that high energy electrons, at least, are present throughout the ISM and within various objects, such as supernova remnants. The GCR represent a significant component of the energy in the ISM and are part of the on-going matter-energy cycle in the galaxy. Thus, understanding the sources and acceleration of these particles remains one of the important unanswered questions in High Energy Astrophysics.

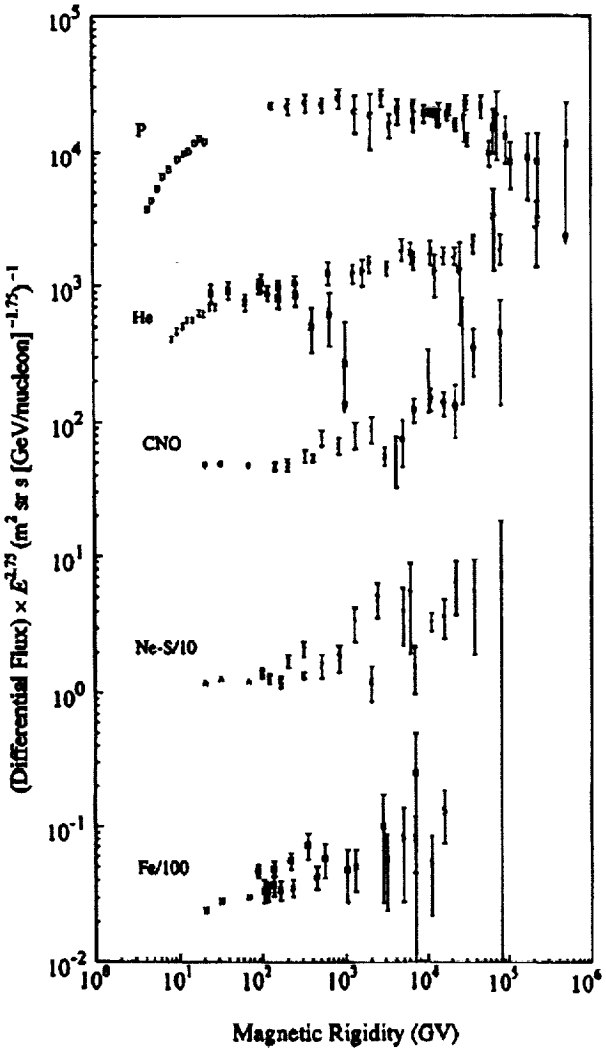

Fig. B.1: Compilation of energy spectra for groups of elements

The results in Figure B.1 come from a variety of experiments, performed over many years, utilizing various techniques, i.e. emulsion chambers or thin calorimeters, transition radiation detectors, ring imaging Cherenkov counters, magnetic spectrometers, or gas Cherenkov detectors, each covering a limited energy interval. Taken together, the data extend up to ~10^{14} eV for protons and to lower kinetic energies for the heavier species. However, the agreement among the experiments is not as good as might be hoped, and the statistical uncertainties at the high energy end remain large. (Note that the flux in Figure B.1 has been multiplied by $E^{2.75}$ in order to flatten the power law dependence.)

Several surprising results emerge from Figure B.1. First, the most abundant species, H and He, appear to have energy spectra that are different; the flux of He relative to H increasing with energy. Above ~50 TeV, the proton events appear to be less abundant, and this led, originally, to a report of a possible bend, or break, in the proton spectrum. (Even earlier, a break at 2 TeV had been suggested.) The heavier nuclei, viewed in charge groups (e.g., C+N+O), show spectra that appear less steep than Helium, and extrapolated (naively) to higher energy, the overall composition of cosmic rays becomes dominated by heavy nuclei. However, a range of power law exponents can be encompassed by the dispersion in the heavy nuclei measurements shown, making such extrapolation problematic. It is this need for better

measurements to understand these spectra that is the experimental rationale for the ATIC investigation.

Concurrently (over the past 15 years), theorists have developed an attractive and convincing theory of diffusive shock acceleration by supernova blast waves that naturally accounts for the essential observed features of most of the relativistic particles in the galaxy. The mechanism of shock acceleration has been directly observed, accelerating particles within the heliosphere, and is believed to be a prevalent process in astrophysical plasmas on all scales throughout the universe. A characteristic of diffusive shock acceleration is that the resulting particle energy spectrum is much the same for a wide range of parameters, or shock properties. This energy spectrum, when corrected for leakage from the galaxy, approximates the observed spectrum of the GCR.

In shock-acceleration, particles pick up a small increment of energy each time they cross the shock boundary in a random-walking (diffusing) process. The maximum energy accessible in a given situation depends on the rate at which the particles diffuse back and forth across the shock (i.e., on the magnetic field) and on how long the acceleration mechanism acts. For a supernova (SN) shock, the time and distance scales are much longer than the scales encountered in the heliosphere, so the corresponding energies are much larger. However, the available acceleration time is limited by the time taken for the blast wave to propagate outward into the ISM and to weaken to the point that it is no longer an efficient accelerator. In the most commonly used form of the theory, the magnetic field near the shock is so turbulent that the particles do not see the average pre-existing magnetic field. In this case, the characteristic energy $E = Z \bullet 10^{14}$ eV, where Z is the particle charge (e.g. Lagage and Cesarsky, 1983). This implies that the composition would begin to change in the energy region around 10^{14} eV, since this is the limiting energy for protons. However, changing the assumed magnetic field topology or field strength or the characteristics of the medium into which the SNR is expanding (Ellison et al., 1994) could result in changing the predicted maximum energy for the accelerated particles. It is important to have reliable, direct measurements to as high an energy as possible to help constrain the parameters in the diffusive shock acceleration model.

It should be pointed out that the connection between GCR and supernova was suggested nearly 40 years ago, based upon energetics. GCR particles are relatively short-lived in the galaxy (circa 10^7 years) and require periodic replenishing. The required energy input into GCR can be accommodated by very few astrophysical objects, with supernova being the obvious choice since only ~5-10% of their output would need to be converted into accelerated particles.

Ground based cosmic ray air shower detectors have studied the "all-particle" spectrum for nearly as many decades. This data reveals that GCR extend many decades further in energy to 10^{20} eV or even higher. This opens, immediately, another question, namely if the SNR "accelerator" cut off at a maximum energy as theory predicts, what is the source (and acceleration mechanism) for these still higher energy particles? Investigations near the limit of the SNR acceleration process can, perhaps, provide some clues to the answer to this expanded question.

It is this relatively recent confluence of (1) theoretical developments in shock acceleration and (2) exciting new data indicating differences in rigidity spectra that has led to renewed interest in high energy cosmic ray measurements, in general, and to the ATIC experiment in particular. However, an experimental advance would not be possible without the development by NASA of the long-duration balloon (LDB) flight capability. It is now possible to fly reasonably heavy experimental payloads for 10-15 days, circumnavigating Antarctica. In the

astral summer (Dec./Jan.) the polar vortex winds are relatively stable and carry a balloon launched from McMurdo station around the pole, returning it "close to" the launch site in 10-15 days. This represents an order-of-magnitude increase in flight time, compared to standard flights in the US or Canada, and makes possible the study of the very high energy GCR flux.

Figure B.2 shows updated spectra for H and He, with the flux again multiplied by $E^{2.75}$. Comparison to Figure B.1 shows that the apparent fall off at the highest energies for protons is no longer prominent, due, mainly, to refined data from the JACEE group, who report spectra consistent with single power laws. However, Cherry et al., 1999, using a maximum likelihood analysis, show that a spectral break above ~40 TeV cannot be ruled out. The statistical significance of the data is just not high enough to draw a conclusion one way or the other. Other analyses (e.g. Zatsepin and Sokolskaya, 1999; Grigorov and Tolstaya, 1999) still favor a spectral break, so this remains an unanswered question.

The spectral fits shown in Figure B.2 still favor a difference in the spectral index for Hydrogen and Helium at the two sigma level, index change = 0.12±0.06. A difference in the spectral indices would, almost certainly, signify two different types of sources or acceleration mechanisms for H and He (e.g. Biermann, 1993; Zatsepin, 1995). However, RUNJOB reported H and He spectra that show the same index. Note the width of the 'band' covered by the measurements. What is needed to understand the spectral shapes is a set of measurements covering the full energy range with a single instrument of demonstrated capability, and this is a major goal of the ATIC investigation.

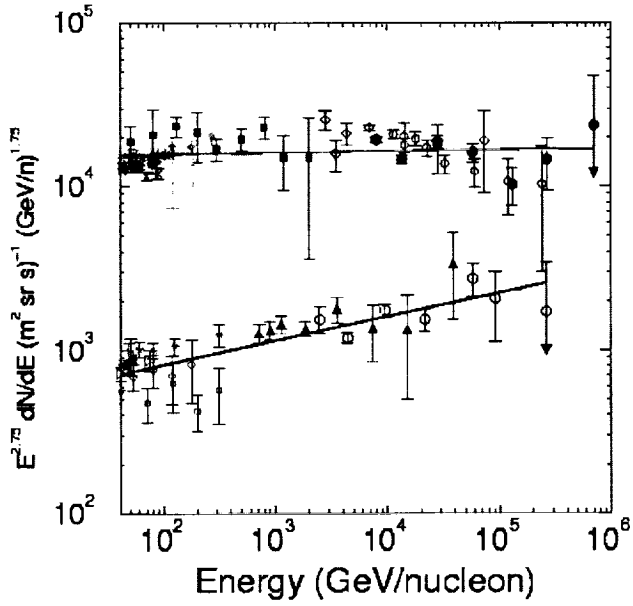

Fig B.2: Compilation of measurement for H (top) and He (bottom)

With the baseline ATIC design described below we will obtain a statistically significant measurement of cosmic rays with energy up to ~10^{13} eV with an exposure of 1-2 days. However, to extend these measurements up to ~10^{14} eV will require several long duration (>10 day) balloon exposures, and ATIC has been designed for such a campaign.

C. The ATIC Concept

1. Ionization Calorimeter

The only practical method of energy determination over a broad energy range for $Z \geq 1$ seems to be ionization calorimetry. In an ionization calorimeter, a particle's energy is deposited inside a medium via a cascade of nuclear and electromagnetic interactions. At each step of the cascade, the energy of the primary particle is sub-divided among many secondary particles. The area under the curve of ionization energy versus depth in the medium provides a measure of the particle energy. In principal, an infinitely deep calorimeter provides energy resolution limited

only by the statistical nature of the cascade process and the measuring technique. The energy resolution of a finite calorimeter, however, depends on the fluctuations in the energy transferred to the pions, particularly in the first interaction. Practical calorimeters for balloon applications must necessarily be limited in thickness, in order to have a reasonable cross sectional area, i.e. geometrical factor, and a "flyable" weight. In a thin calorimeter to measure GCR, the primary nucleus must undergo at least one inelastic interaction; and deposited energy must be measured with good resolution. An optimal thin calorimeter would employ a target with thickness of about one proton interaction length located upstream of a calorimeter which, in turn, must be thick in radiation lengths ($\geq$ 10 r.l.) to develop the cascades ensuing from the interactions.

For ATIC, we developed an advanced calorimeter based upon fully active Bismuth-Germanate (BGO) scintillating crystals (1.12 cm per r.l.) following a 30 cm carbon target (25 cm per r.l.). The incident particle interacts in the carbon, but the majority of the shower develops in the BGO. On our first LDB flight from McMurdo, we flew eight layers of 2.5 cm thick BGO crystals giving a calorimeter depth of 17.9 r.l. vertical, sufficient to contain the shower maximum for the energies of interest.

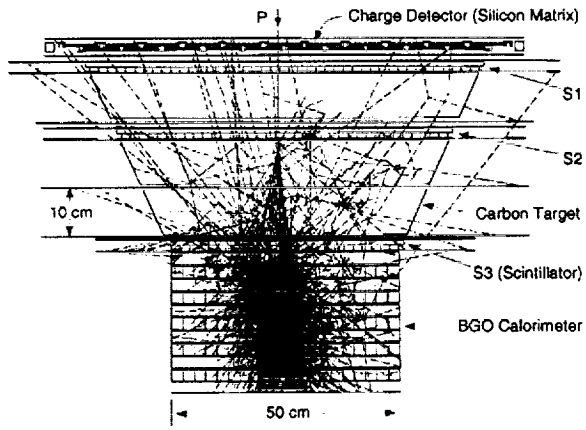

Fig. C.1. An example of proton shower in the McMurdo flight configuration

The instrument must also determine the charge of the incident particle and measure its trajectory through the apparatus. A schematic of the ATIC instrument is shown in Figure C.1. Crossed strip scintillator layers (S1-S3) are located at the top, bottom and within the carbon target to provide triggering (geometry definition) as well as a measure of the trajectory of the incident cosmic ray, combined with the location of the shower core from the calorimeter. At the top of the instrument is a silicon detector to determine the charge of the incident particle. In a calorimeter, there is always some "backsplash" of particles emitted into the backward hemisphere that can confuse the charge measurement. To resolve this problem, the Si-detector is pixelated, which allows separation of the backscatter from the incident particle.

ATIC has been designed specifically as a LDB payload, meeting stringent weight requirements and launch conditions. Telemetry, once out of line-of-sight communications, is very limited, requiring both on-board data recording and semi-autonomous operations. The payload is contained in a pressure vessel and utilizes photovoltaic arrays for power. Moreover, since we plan to fly ATIC multiple times, it must be protected from disastrous landings, as well as being easily disassembled for field recovery. Developing such a "re-usable" balloncraft has presented enormous challenges for ATIC (Guzik et al., 1996, 1999).

The ATIC team simultaneously developed the hardware systems (described later) and simulated the performance of the overall instrument through Monte-Carlo studies (Seo et al., 1996; 1997). These latter are described in the next section, followed by a summary of the validation studies performed at the CERN SPS accelerator.

2. Simulating the Performance of ATIC

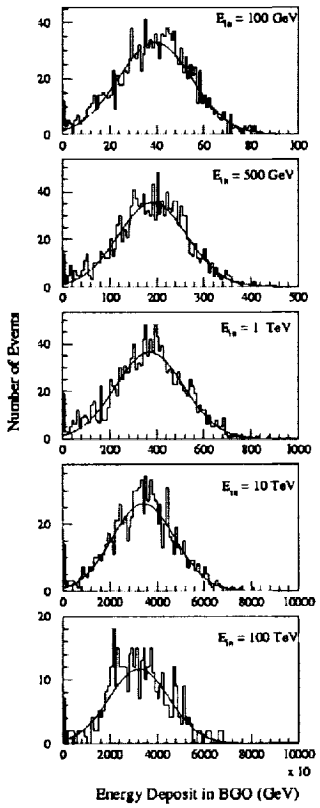

Fig. C.2: Energy deposition in 20 cm depth BGO calorimeter for 10^2, $5x10^2$, 10^3, 10^4, and 10^5 GeV protons.

The detector simulations to understand the physics involved in high-energy cosmic-ray particle detection and to investigate the methods of data analysis have been led by the University of Maryland. A simulation model, based on the GEANT (Brun et al. 1984) code has been developed for simulating nuclear-electromagnetic cascades initiated by protons, He, and heavy nuclei to trace cosmic ray particles through the full detector system, following the event interaction, shower development and back scattered particles. Calculations for both isotropically and vertically incident particles have been carried out from 10^{10} to 10^{14} eV total energy: a few primary energies per decade. Calculations with a power law in energy with threshold 5 GeV, which represents the actual cosmic ray flux, were also carried out. The experimental configuration was modeled as realistically as possible including dead material, gaps and mechanical structure. An example of a simulated proton event in the McMurdo flight configuration of the ATIC instrument is shown in Fig. C.1. The isotropically incident data sets have been used to understand the background events, the detection efficiency, and the instrument performance (Wang, et al. 1997). Based on isotropically incident protons following a power law in energy in the McMurdo flight configuration, the trigger model has been optimized to decrease the background level and increase the detection efficiency.

Energy Resolution: The distributions of energy deposited by isotropically incident protons in the BGO calorimeter (8 layers for the McMurdo flight configuration) for 10^2, $5x10^2$, 10^3, 10^4, and 10^5 GeV protons are shown in Fig. C.2. The simulated results presented here were obtained by selecting all particles that have their first interaction anywhere in the carbon target. The mean energy deposit as a function of the BGO thickness for a range of energies from 100 GeV to 100 TeV is shown in Fig. C.3. The mean of the energy deposition distributions (Em) and the energy resolution (the ratio of the standard deviation (σ) of the energy deposit distribution to the mean energy deposit) are shown as a function of the incident energy

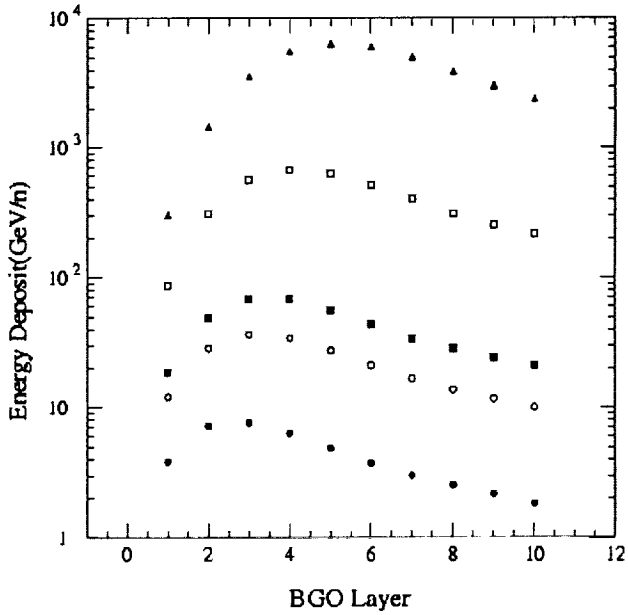

Fig. C.3: Longitudinal shower profile of 10^2, $5x10^2$, 10^3, 10^4, and 10^5 GeV protons.

in Figs. C.4a and C.4b, respectively. The mean energy deposit of protons is about 40% of the incident energy, essentially linear with the incident energy. The energy resolution is about 40% and nearly energy independent. The change in resolution with energy distorts the true input spectrum. However, since the measured spectrum is a convolution of the actual input spectrum with the detector resolution, the true input spectra can be obtained by deconvolution. For heavy-ions, the energy resolution is much better than for protons (Seo et al., 1996). The heavy ion simulation model is described in Kim et al. (1999).

Charge Resolution and Backscatter: Backsplash from the calorimeter is a rather widely accepted explanation (Ellsworth et al. 1977) for confusing proton and helium nuclei and causing

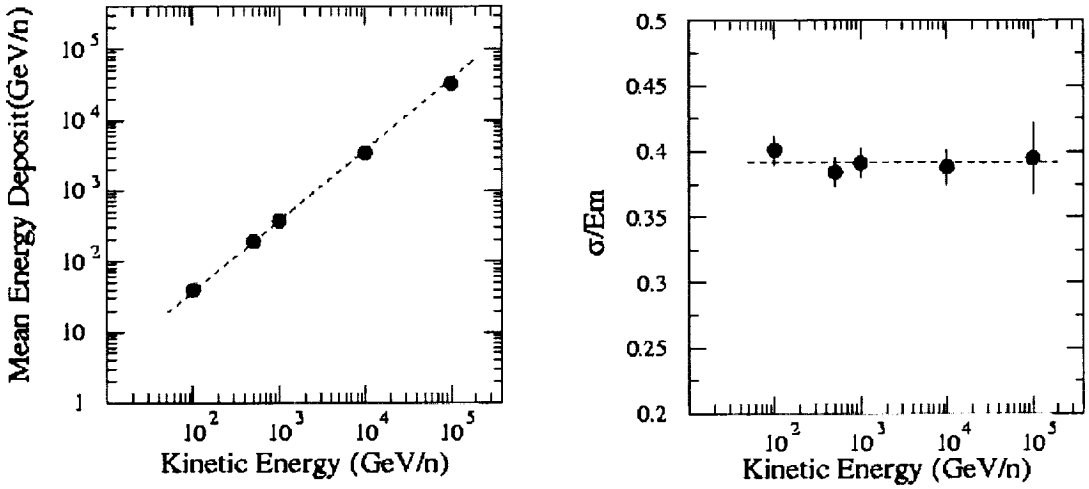

Fig. C.4: Energy dependence of the proton mean energy deposit and the energy resolution.

a proton spectral bend in previous experiments. These albedo particles consist mostly of relativistic (several MeV) electrons that result from gamma rays scattered into the backward hemisphere of the calorimeter. They also include non-relativistic particles, which may result either directly from nuclear interaction products emitted into the backward hemisphere or from albedo neutrons produced in the interactions. The simulations track the backscattered particles from the calorimeter/target to study how these albedo particles can affect the primary charge measurement. Without any segmentation in the charge measurement device, Si or S1, the output signal would include all the energy deposited anywhere in Si or S1, including the energy deposited by the backscattered particles. For this case, at 1 TeV most (80%) of the protons would be misidentified as heavier particles due to the albedo contamination. This problem can be reduced significantly by segmenting the Si and S1 detectors.

For example, with 10×10 cm^2 segmentation, only 11% of 1 TeV protons would be misidentified, and this reduces to 1% with $2 \times$

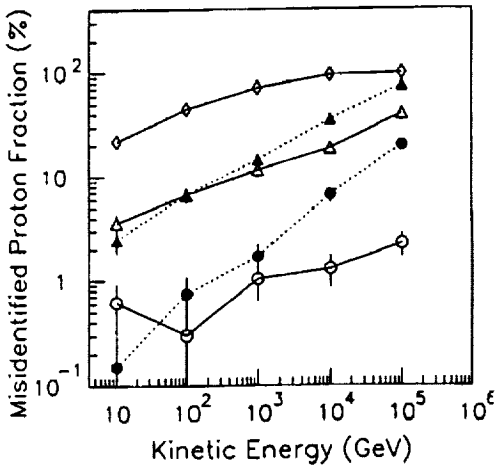

Fig. C.5: Fraction of misidentified protons versus incident energy.

2 cm^2 segmentation. At 100 TeV, the energy deposit in a single scintillator strip located at the incident position is about 2.5 Minimum Ionizing Particles (MIPS) on average, but it can be as high as 20 MIPS (0.1% probability). By studying the energy deposit in S1 at several energies, the magnitude and variation of the fraction of misidentified particles with energy was obtained (Fig C.5) for five different configurations, from bottom: (1) 2×2 cm^2 pixels (2) two crossed 1 cm thick 2 cm wide strips, (3) 10×10 cm^2 pixels, (4) two crossed 1 cm thick 10 cm wide strips, and (5) without segmentation.

We have simulated the impact that residual errors from backscatter (protons being misidentified as heavies) would have on the measured energy spectra. For the ATIC configuration comprised of a Si Matrix with 1.5×1.9 cm^2 pixels, backscatter effects are not expected to steepen the spectral index by more than 0.01. We note that the albedo effect is reduced if the charge measuring layers, S1 and Si, are farther from the calorimeter.

Trajectory Resolution : The cross-stacked BGO layers give measurements of each cascade axis coordinate, x and y. By extrapolating the linear fit of the cascade axis coordinates to Si and S1, the entrance particle position was calculated. The deviation between the actual incident position and this measured position in S1 is shown in Fig. C.6, for protons having vertical incidence at an energy of 1 TeV. The position resolution is 0.54 cm. Adding the information from the scintillators between the carbon layers gives additional cascade coordinate measurements, and improves the resolution by ~20% (Ganel and Seo, 1998). The position resolution is better at higher energies since the cascade core is better formed at higher energies, i.e., the forward momentum is higher in comparison to the transverse momentum, and that helps to collimate the showers.

The better the position resolution the smaller the circle of confusion in Si, which increases the probability that the incident track can be localized within a single detector in the charge module. This gives better backscatter rejection. For a 1 TeV proton, the resolution is 0.54 cm, so the three-sigma circle of confusion has a diameter of about 3.2 cm. A single Si pixel located at the calculated position won't give the correct charge measurement, because the incident particle could also be in either of the neighboring pixels. By considering the closest neighboring pixel in addition to the pixel at the calculated position within the circle of confusion, more accurate charge measurements can be made. In actual data analysis, all detectors within the circle of confusion must be examined, and the one containing the largest signal must be assumed to contain the incident particle's track. The best results will be obtained when the detector segmentation is smaller than the circle of confusion as is the case for ATIC.

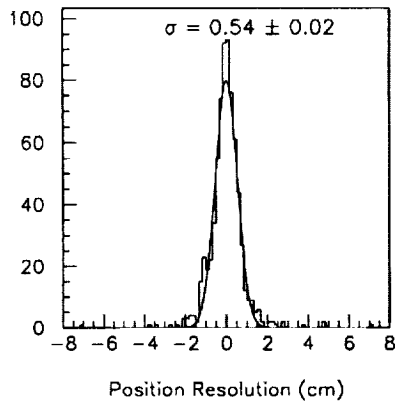

Fig. C.6: Trajectory resolution in S1 calculated from the BGO shower profile for 1 TeV protons.

D. ATIC Instrument Development

During 1999 a version of the experiment, very similar to the flight version, was assembled and taken to the CERN particle accelerator facility in Geneva, Switzerland to test the experiment concept and obtain a performance evaluation. Following the CERN runs, the payload was

returned to LSU where we incorporated the "lessons learned" at CERN into the experiment in preparation for its first balloon.

1. Validation at the CERN Accelerator

During August / September, 1999 the ATIC experiment was shipped to CERN where it was exposed to high energy proton, electron and pion beams. The experiment configuration used as well as the results from these tests is discussed below.

Experiment Setup: The ATIC experiment is sketched in Figure D.1, with the major components indicated, and photos of the experiment in the CERN beam line are shown in Figure D.2. The top most detector is the silicon matrix developed by NRL / MSU which is designed to provide an accurate measure of the incident particle charge over the charge range 1 to 28 for incident angles up to 57° in the presence of backscatter from showers in the calorimeter (Adams, et al., 1999a). For flight this detector consists of 4,480 reverse-biased silicon diode "pixels" each of which is 380±5 μm thick and of dimensions ~1.5 cm by ~1.9 cm. Four such pixels are arranged on a ceramic "daughter board" which has a dimension of 3 cm by 6 cm. In turn, one "mother board" of dimension ~6.6 cm by 111 cm carries 28 daughter boards and seven 16 channel application-specific integrated circuit (ASIC) CR-1 chips (Adams, et al., 1999b) to provide a multiplexed readout of the 112 pulse heights. Two mother boards slide into an aluminum "rail" with one inverted over the other and offset by half a pitch to provide a "ladder" with active area 6 cm by 100 cm. On the bottom structural honeycomb panel 10 ladders are arranged and another 10 ladders are offset by half a pitch and attached to the top panel to provide a detector with active area about 99 cm by 111 cm. Four "grandmother boards" provide the ADCs, calibration sources and the logic necessary to readout the detector. For CERN three ladder systems populated with about 120 daughter boards each were available for testing. This provided an active area of about 17 cm by 70 cm centered on the aperture with the long axis arranged vertically, i.e. perpendicular to the experiment rotation axis (see Figure D.2a). Except for the reduced area, the detector configuration and readout electronics were those anticipated for flight, allowing an effective evaluation of the detector.

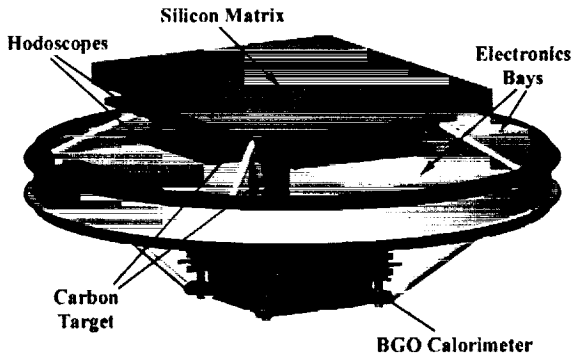

Fig. D.1: Schematic of the ATIC experiment

The target section below the silicon matrix has about ¾ of a nuclear interaction length of material, mainly three 10 cm thick layers of carbon, but this represents few radiation lengths, so that for an interacting particle, the shower development in the target section is minimized. Further, the target section includes three plastic scintillator strip hodoscopes to provide the experiment with a fast trigger that defines the aperture, and auxiliary measurements of the incident particle charge and trajectory. The three hodoscopes (S1, S2 and S3) are of similar construction and are composed of Bicron BC-408 plastic scintillator strips 2 cm wide by 1 cm thick. To maintain a ~24° opening angle, each hodoscope has a different active area. For S1 there are 42 strips of length 88.2 cm in each layer, while 35 strips of length 74.2 cm comprise each S2 layer and 24 strips 52.4 cm long make up S3. Each hodoscope module has two layers

oriented by 90° to provide a X-Y measure of the particle "hit" position. The strips are wrapped in aluminized mylar and on each end is glued a UVT Lucite transition and a Hamamatsu R5611 photomultiplier tube (PMT). For the scintillator strip readout, the PMT bleeder base utilizes two dynode pickoffs to cover the required dynamic range (~0.5 MeV to 800 MeV). The PMT anode is used to provide a fast "pre-trigger" signal, and a test LED is incorporated directly into the PMT base. These signals are wired directly to a Front End Module (FEM) board that contains

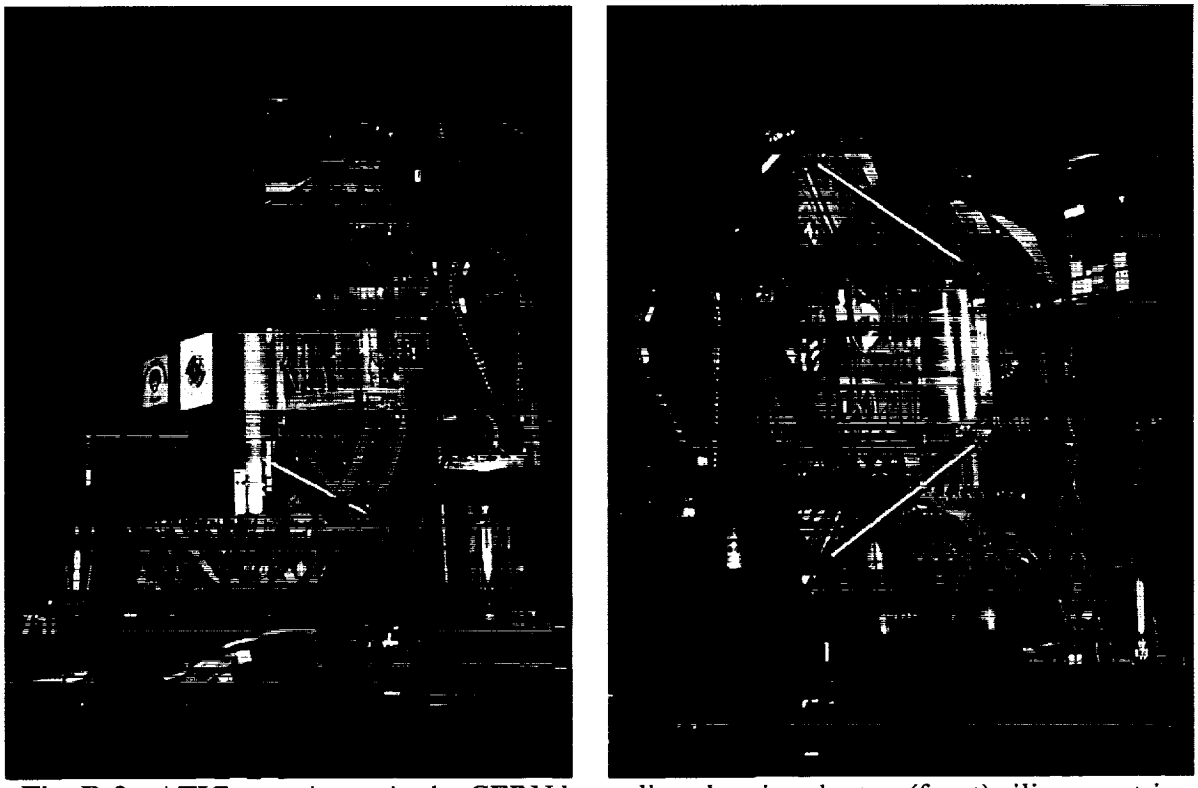

Fig. D.2: ATIC experiment in the CERN beam line showing the top (front) silicon matrix detector (left panel) and the bottom (back) calorimeter stack (right panel)

six ASIC chips based on the design used for the ACE mission. Each ASIC has 16 input channels and outputs two "trigger" signals as well as 12 bit digitized pulse heights.

In an ionization calorimeter, a particle's energy is deposited in an absorber via a cascade of nuclear and electromagnetic interactions. In ATIC, the calorimeter is located below the target section, and, for CERN, was composed of a stack of 10 trays with forty 2.5 cm by 2.5 cm by 25 cm BGO crystals in each tray. Thus, the calorimeter was about 22 radiation lengths (~1.14 nuclear interaction lengths) in depth. Each crystal is viewed, through an air gap, by a single Hamamatsu R5611 PMT. The PMT bleeder string base incorporates a three dynode pickoff to cover a dynamic range of energy deposits from about 10 MeV to about 20 TeV and is designed for low power consumption. The PMT and bleeder string electronics is wrapped in brass foil for electrical shielding and the dynode signals are wired to a FEM board that is almost identical to the hodoscope FEM. These calorimeter FEMs also use the ACE ASIC. LEDs are incorporated into the front end electronics so each PMT can be checked for liveness and stability.

The BGO calorimeter stack can be seen in the right hand panel of Figure D.2. Each layer is rotated by 90 degrees to provide an X-Y coordinate for determining the shower core trajectory, using the techniques described in Ganel et al., 1999. The black vinyl coated handles are used in

tray handling (each tray weighs close to 50 kg), and the PMT / FEM boxes can easily be mounted / dismounted on the tray ends. We adopted this design to assist in the recovery of this critical detector system following a LDB flight in Antarctica.

Surrounding the detector stack, electronics bays hold the flight computers, readout electronics, power system boards and other instrument electronics. Cabling from the connectors on the FEMs for both the hodoscopes and calorimeter trays run to the electronics bays where the remainder of the readout electronics is mounted.

Finally, on each of the four corners three struts transfer the loads of the experiment through the pressure vessel ring to an external structure (Figure D.1) that attaches to the balloon. For CERN the same internal structure attaches to the rectangular steel frame which is motorized so the entire experiment could be rotated about an axis that is perpendicular to the beam axis. This allowed us to adjust the pitch of the experiment to vary the angle by which beam particles are incident on the ATIC detectors. This entire apparatus was mounted on a table which could move vertically or horizontally. In this fashion we were able to collect data with beams at different positions on the detector stack and at different incident angles.

The actual beam exposure took place between Sept. 1 and Sept. 7, 1999 with ATIC located in the H2 beamline and using facilities provided by the CMS experiment area. Over this time period ATIC acquired beam for close to 50 hours. The beams included 100 GeV, 150 GeV and 300 GeV electrons; 150 GeV and 375 GeV protons; and 150 GeV pi-minus. For all of these beams ATIC was positioned "face-on" to the beam as shown in Figure D.2 so that the energetic particles would pass through all detectors at normal incidence. ATIC was also pitched upward to collect data at 15^{o} and 30^{o} incident angles. Further, measurements were made with ATIC positioned so that the beam would pass through the center as well as the four calorimeter quadrants. In addition, with a few beams we "walked" the experiment over a fine vertical scale to provide an intercomparison of the silicon, hodoscope and calorimeter segments. Finally, a few specialized runs were performed to study the effects of side entering events on the trigger logic and to examine how interactions above the silicon matrix would affect charge resolution. Much of the information in this rich dataset is still being extracted, but some of the important performance parameters for ATIC are discussed below.

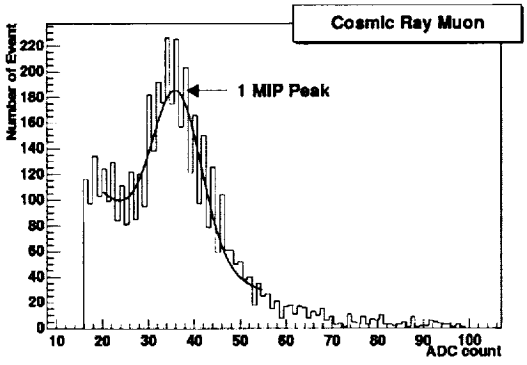

Fig D.3: Cosmic ray muon data

Current Results and Comparison: ATIC performance parameters have been derived from Monte Carlo simulations, but we need to anchor such results with real particle data i.e. CERN accelerator beams. These runs provide functional verification of the ATIC detectors, as well as verification of the simulation model, which must be relied upon to extrapolate the response to the higher energy cosmic rays observed during the balloon flights.

For the September 1999 run cosmic-ray muons were also measured, and special runs of pedestal, charge-pulser and LED flasher events were collected for calibration purposes. For all beam particles ATIC was triggered externally, using CERN-provided scintillator paddles and trigger electronics. For cosmic-ray muons the ATIC pre-trigger was utilized (S1-S3 coincidence).

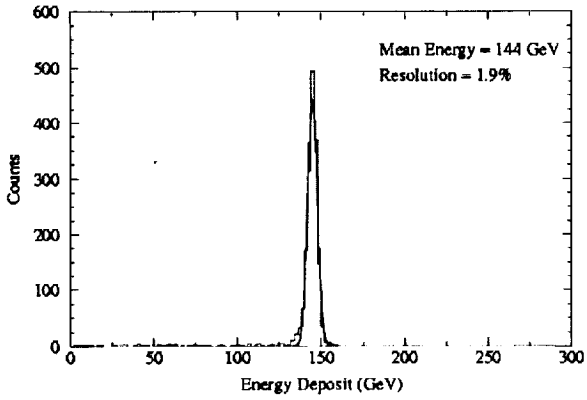

Fig D.4: Energy deposit in BGO for 150 GeV electrons

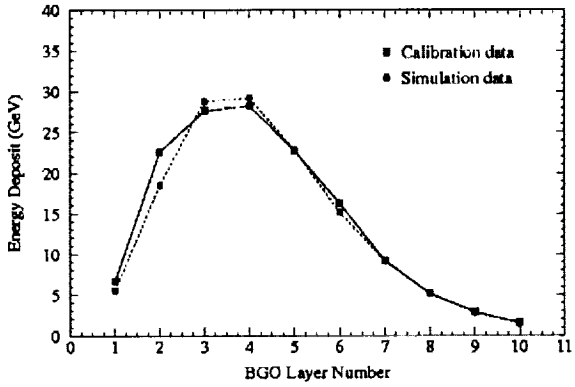

Fig D.5: Shower profile of 150 GeV electrons. Circles are simulation results, Squares are measurements

The data was written by the Flight Data System (FDS) in binary format on a PC running under the QNX real-time operating system. The binary files were read using a ROOT-based custom package – the ATIC Data Processing System (ADPS). ROOT was developed at CERN (Brun and Rademakers, 1997) and is a powerful, object-oriented, data analysis and presentation tool. Using ADPS the data processing team extracted the pedestal values for each electronic channel. After the pedestal subtraction, cosmic-ray muon distributions were plotted and fitted for each BGO crystal to provide a calibration for the calorimeter's low-range readouts. Figure D.3 shows an example of cosmic-ray muon data that was used for calibration of the low-range of the calorimeter. These provided the inter-crystal calibration for most crystals. By comparing with our muon simulations, 1 MIP energy was assigned to the ADC counts where the 1 MIP peak is located. In this way, ADC counts were converted to physical units, i.e., MeV. Events with showers were used to extract the inter-range calibrations for the mid-range and high-range. With the pedestal and gain corrections handled, the calibrated data was analyzed.

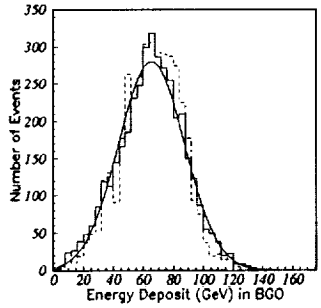

Fig D.6: BGO energy deposit for 150 GeV protons. Data plus gaussian fit (solid), Simulations (dashed).

Prior to the run, the team simulated the expected beam conditions (particle types, energies, locations and angles). These simulations have been used to validate the data collected at CERN. Beams were simulated both as infinitely thin beams and as a more realistic 2 cm diameter beam. As shown in Figs. D.4 and D.5, the electron energy resolution is about 2% at 150 GeV, and its shower profile

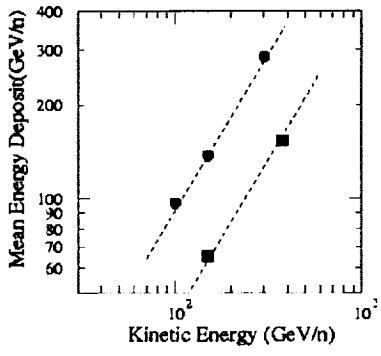

Fig D.7: BGO mean energy deposit for electrons (circles), & protons (squares).

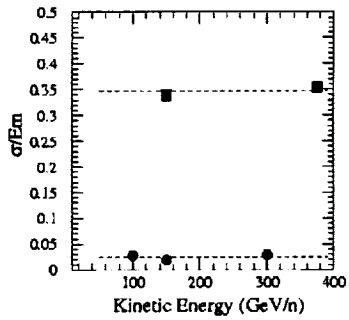

Fig D.8: Energy resolution of electrons (circles), protons (squares).

agrees well with the simulations. The proton data also show a good agreement with the simulations as shown in Fig. D.6. In this plot, we have used a simple trigger and event selection algorithm to select particles that interacted in the carbon target. The CERN calibration data sets are summarized in Figs. D.7. and D.8. The energy response and resolution are nearly energy-independent, to the limits of the CERN data. The mean energy deposit of protons is about 40% of the incident energy, essentially linear with the incident energy. The energy resolution for protons is about 35% and nearly energy independent. We note here that the CERN calibration utilized 10 layers of BGO. For the Antarctic configuration, which has 8 layers of BGO, the resolution will be about 40%.

2. Flight Systems

Following the fall, 1999 CERN calibration, the ATIC team prepared the instrument for flight. This involved isolating and repairing detector and readout electronics issues uncovered during the CERN testing, completing the mechanical structure design and fabrication and finalizing the experiment control software. During this process, a detailed mass analysis determined that the experiment as configured for CERN was about 300 to 500 pounds over the McMurdo LDB launch limit. Thus, a significant program of mass reduction was undertaken. Below we describe the ATIC flight systems.

Detector and Readout Electronics: Since the hodoscope and calorimeter subsystems were tested in a configuration similar to that for flight, most of the effort on these detectors has focused on repairing problems identified at CERN and on weight reduction measures. For the calorimeter we discovered a few miswired channels in the electronics and about half of the LED pulser circuits would not fire correctly when commanded. The pulser problem was corrected by changing a capacitor that controls the pulse timing and the miswired channels were fixed. In addition, for all 400 calorimeter segments we have readjusted the relative gains between the PMT dynode outputs to provide higher energy resolution in the low energy range and included a custom light attenuator for each crystal - PMT pair. The amount of attenuation is adjusted so that each BGO/PMT pair outputs roughly the same ADC value for a minimum ionizing particle.

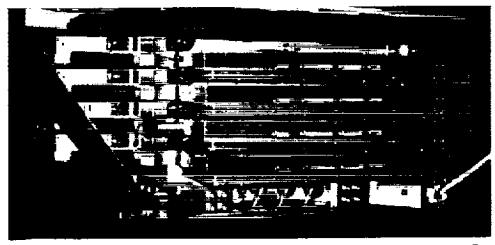

Fig D.9: The flight calorimeter stack

The BGO calorimeter is designed as a modular system with each layer consisting of a tray of 40 BGO crystals plus two "FEM Boxes" that are attached to the open ends of the tray. A calorimeter stack of eight layers is shown in Figure D.9. The "FEM Box" contains all the front end readout electronics plus connectors to route control and data lines. An FEM Box slides onto a pair of tray "fingers" and is fixed in position by two extended length, knurled knob screws. Trays are provided with handles and can be easily added or subtracted from the stack. This modular design was adopted for two reasons. First, we can change the stack configuration (without any redesign work) to take advantage of, or conform with, weight constraints associated with different launch sites. For example, while we anticipate the McMurdo configuration will include eight trays, a potential Fairbanks LDB configuration can include ten trays. Second, the modular tray design facilitates calorimeter recovery from Antarctica following a McMurdo flight. The tray handles and FEM Box attachment screws were specifically designed to be used by a recovery team in full arctic gear.

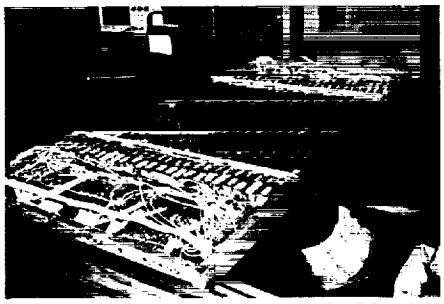

Fig D.10: S3 hodoscope half with Gatorfoam structure

The plastic scintillator S1, S2 and S3 hodoscopes performed well at CERN with only a handful (~15) of the over 200 segments needing repairs. Most of the problems were located in the PMT bleeder string electronics, but in a few cases the PMTs needed to be replaced. These repairs were completed and strips were mounted on a "gatorfoam" structure to reduce weight (Figure D.10). Gatorfoam, from International Paper, consists of a rigid polystyrene foam core bonded on both sides by a smooth, moisture resistant man-made wood fiber veneer. This product has previously been used as a aluminium honeycomb replacement on balloon payloads such as ISOMAX and, in our case, provides an average 26% weight reduction. Each hodoscope half includes the front end readout electronics necessary to digitize the signals from all PMTs on both ends of the strips as can be seen in Figure D.10. The two halves are oriented at right angles to each other and attached to form a single detector module. Like the BGO layers all three hodoscope modules were designed to be easily recovered following an LDB flight.

Fig D.11: Twelve of the 112 Silicon matrix pixels on a motherboard

Since the CERN runs, 40 more motherboards for the Si-matrix have been made and populated (c.f. Fig. D.11). The mechanical structure has been re-designed to reduce weight and the new structure has been completed. Testing of the new motherboards was completed. The exact locations of the daughter boards on all motherboards must be measured for use in data analysis. This followed by a careful ground calibration of all 4480 detector pixels in the matrix using a precision charge injection source. This is the fundamental calibration that will allow data from all pixels to be combined on a common scale.

The ATIC detector readout uses a series of custom electronic boards that were designed, developed, debugged during the past several years and tested at CERN. The boards which make up the readout chain are illustrated in Figure D.12 and include A) the Detector Interface Module (DIM) which provides the interface between the Detector Control Unit (DCU) computer and the readout chain, B) the ASIC Control Logic Board (ACLB) which interfaces to the trigger logic, controls the details of the detector readout and provides for data sparsification, and C) the Front End Module (FEM) which includes the ASICs used to read and digitize the detector signals, the LED and charge pulser calibration circuits and the circuitry that collects the front end trigger signals. For the hodoscopes and calorimeter, the FEM boards are identical and incorporate an ASIC almost identical to that used by the ACE SIS experiment. For the silicon matrix the FEM functionality is divided between the "mother board" (MB), which includes the CR-1 ASIC, and the "grandmother board" (GMB) which incorporates a 16-bit multiplexed ADC. We currently have sufficient spare "ACE" ASICs to repopulate all hodoscope and calorimeter FEM boards if necessary and an equivalent number of CR-1 spares for the silicon matrix. Most of the "logic" circuits for the DIM and

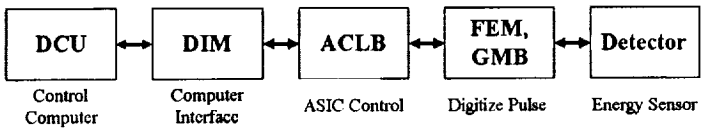

Fig D.12: The ATIC detector readout chain electronics

ACLBs are encoded within ACTEL FPGA chips. This approach allows some flexibility to enhance the DIM and/or ACLB capabilities, if required, during the flight program without the need to alter the circuit boards.

At CERN, proto-flight versions of the DIM, ACLB, FEM and silicon matrix electronics along with an initial version of the experiment data acquisition software were used to read the ATIC detectors. This CERN environment placed considerably more stress on the system than we would expect with a cosmic ray "beam". However, we were still able to achieve a maximum rate of about 120 events per spill (~70 Hz) with average event record sizes in the range of 2 kilobytes. Further, in this environment we were able to uncover several timing, handshaking and software bugs which have since been fixed and may not have been otherwise revealed until the first ATIC test flight. As a result we now have a very high confidence that the readout electronics is ready for flight.

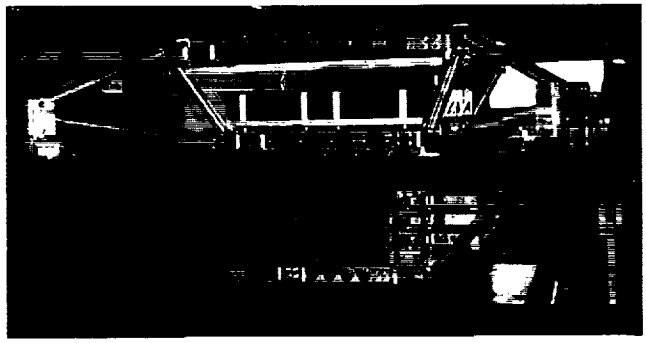

Fig D.13: The detector internal support structure

Mechanical Structure: Much effort post-CERN, was devoted to completing the fabrication of the payload support structure and to implementing measures that would reduce the overall mass relative to the configuration taken to CERN. The full ATIC mechanical structure was examined using finite element analysis (FEA) modeling and, in consultation with the NSBF, designed to support the expected stress at the minimum weight. Figure D.13 shows the flight internal structure with the calorimeter stack on the bottom and the carbon target section on the top. The detectors are supported by three struts on each of the four corners of the experiment. The bottom set of struts provide the primary support for the calorimeter. To add or subtract layers from the calorimeter these struts would need to be of different length. Currently, we have struts for calorimeters with 8, 9 or 10 layers. The upper two struts support the target section independent of the calorimeter. Lateral support bars running down all four corners align the calorimeter with the target section and keep the BGO layers from shifting under lateral loads. All support struts connect to an internal load pad which, in turn, is bolted through the pressure vessel ring to external load pads that attach to the external structure.

Fig D.14: ATIC external structure

The external structure is shown in Figure D.14. The main pressure vessel ring is in the middle of the photo, the balloon train attaches to the NSBF supplied rotator at the top apex of the structure, and the SIP hangs below the square platform seen in the bottom third of the figure.

The platform also provides a connection point for ballast hoppers, and is where items such as batteries and / or the photovoltaic (PV) charge controller can be located. The PV arrays will be mounted on struts that clamp to and extend from the structure. This structure is fabricated from aluminium tubing with eyelets at each end of the tubes which are, in turned, pinned to connectors. The structure is resting on a steel frame fitted with oversize casters to allow us to

move the experiment on the ground. Prior to flight this steel frame is removed and crush padding is attached to the four "landing legs". The entire structure can be easily assembled or disassembled and also provides some protection for the experiment if (when) the payload tips over on landing.

The internal structure with detectors (Fig D.13) fits within the external structure ring and pressure vessel hemispheres are attached on the top and bottom. The pressure vessel is a ~91" diameter sphere with a Kevlar fabric outer layer for strength and a polyurethane inner layer to provide the pressure seal. Similar pressure vessels have already been flown during the ISOMAX project. The pressure vessel in hand at LSU has been proof pressure tested to ~17 psi and a leak rate of $< 2 \times 10^{-4}$ psi per hour at 10 psi has been measured. At this leak rate we would lose less than 0.1 psi during an extended 15 day LDB flight. To be safe, however, our first flight, at least, will include a simple gas make-up system.

Table 1: ATIC Mass Estimate

Component	Mass (lbs.)
Silicon Matrix	90
Hodoscopes	191
Graphite Target	596
BGO Calorimeter	1017
Electronics	96
Internal Structure	200
External Structure	613
PVs, Batteries, Gas	205
Experiment Total	**3008**

Table 1 lists the mass budget for the major components making up the ATIC experiment. Thus, the total ATIC science weight given in Table 1 is within the launch constraint for a McMurdo LDB flight. Launch weights for a Fairbanks LDB are 500 pounds larger.

Power System: The ATIC power system uses a 28V input, supplied by either Lithium cells (for ConUS) or a PV array (for the LDB), to generate and distribute power to the flight data system, readout electronics and detectors. The system also includes latching relays so that discrete commands can be used to power on / off the computer control systems, and power controllers for software commanding the readout electronics and detector high voltage power. In addition, all critical voltages and relay states are monitored and transmitted to the ground in the housekeeping telemetry stream. Finally, the system includes some redundancy for critical systems like the primary flight control computer.

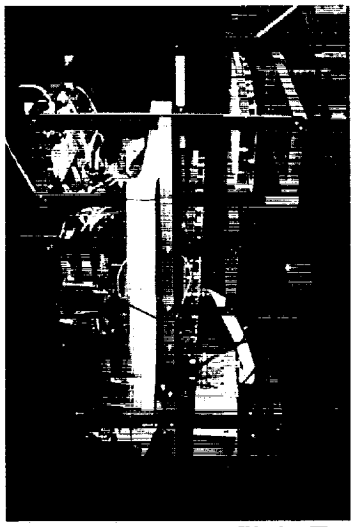

Fig D.15: ATIC flight E-bays & power system

The power system, the flight data system and the detector readout ACLBs, are housed in four electronics bays (E-bays) that surround the middle section of the ATIC detector stack (see Figure D.2). Following CERN the E-bays were redesigned to enhance access to the ACLBs and to reduce the overall weight. These are shown in Figure D.15 with all four E-bays stacked vertically for bench testing. During the redesign we consolidated some flight software functions allowing a PC-104 stack to be removed, reduced the power supply redundancy to critical systems only, and rebuilt the E-bay structure using PVC angle. This refined design represents a mass reduction, relative to CERN, close to 50%.

The power consumption for all major ATIC subsystems is listed in Table 2 and is based upon or scaled from measurements made with flight components. The expected power consumption is well within the power provided by the PV system. Two PV arrays, each have an

area of 56 ft^2 and together provide more than 650 watts of power. This provides sufficient residual power to operate internal heaters for thermal control.

A steady-state thermal analysis has been conducted for the ATIC science-payload in flight configuration. ATIC utilizes a spherical pressure-vessel assembly, with a covering insulation layer (~3 cm fiber-glass) to provide a passive thermal control system, maintaining interior air temperature between 10 and 20°C, at 1 atm pressure. An effective internal conductance coefficient (combined for natural convection and conduction in air) of 5 W/m^2K was used, as well as an external convection coefficient of 0.4 W/m^2K. External structural members are painted white. However no effect of these, or interaction with the SIP module have been included in the thermal analysis. Our insulation is a duct-type fiberglass insulation, chosen largely for its lightweight (0.75 lb/cuft). We had absorption and emissivity measured at an independent testing laboratory, resulting in average values of absorptivity = 0.3, and emissivity = 0.88. Thermal conductivity has been assumed to degrade by 15% because of the near vacuum conditions encountered during flight. Worst-case cold/hot conditions have been calculated, based on limits of solar, albedo and earth-IR.

Table 2: ATIC Power Estimate

Component	Power (W)
Silicon Matrix	70
Hodoscopes	44
BGO Calorimeter	52
Flight Data System	158
Fans / Heaters	60
Experiment Total	**384**

Fig D.16: The DCU with a ACLB and FEM

Flight Data System and Control Software: The ATIC Flight Data System (FDS) controls the experiment during flight operations including receiving and processing uplinked commands, acquiring and archiving the instrument data, as well as downlinking status information and a small sample of event data. The FDS consists of four modules, with each module assigned a particular control operation such as power and housekeeping (Power Control Unit - PCU), data archive and telemetry (Data Archive Unit - DAU), detector (Detector Control Unit - DCU) and flight control (Flight Control Unit - FCU). All modules run the QNX real-time operating system which is POSIX complaint and facilitates programming across a distributed environment. Flight software processes on different modules communicate across an internal payload ethernet using a client / server message passing scheme. The software is event driven where the "events" are classified as particle triggers, timeouts, commands and messages.

Each module stack is built from available PC/104 "Intel class" CPU, I/O, and peripheral control cards. An example of one such stack can be seen in Figure D.16 which shows the DCU during bench tests and software development. The DCU controls the detector subsystems and reads out the particle event data. The figure shows the custom DIM boards integrated into the DCU as well as an ACLB and FEM mounted in the background. The FCU interfaces with the NSBF SIP to receive uplinked commands and downlink status information as well as with the FDS power control. The FCU "manages" the other FDS modules; decoding commands and distributing them, watching for units that may need to be reset, and collecting status data for downlink. The PCU manages and monitors the detector electronics power system and includes

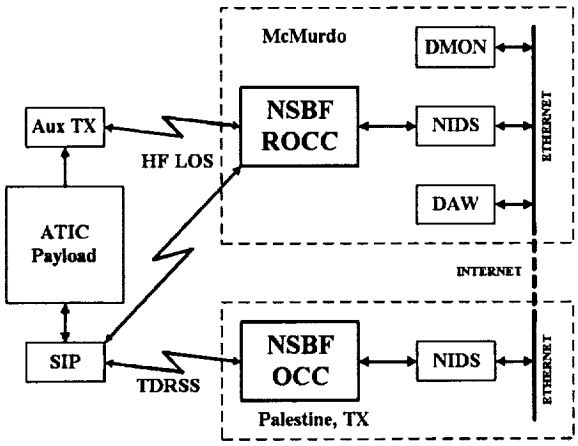

Fig D.17: The ATIC Ground Data System

the processes that collect the voltage, pressure and temperature information for housekeeping records. Finally, the DAU controls the on-board recording of all data to a 50 Gigabyte SCSI hard disk as well as transmitting a portion of the data to the ground during times when the payload is within line-of-sight (LOS). During flight the data rate will be limited to <50 Hz, which given our estimated event record size, will result in a ~50 Gbyte dataset for one LDB flight. A small portion of this data may also be downlinked at a rate of about 4 kbps whenever a TDRSS link is available.

The ATIC Ground Data System (GDS) is illustrated in Figure D.17. The GDS consists of three major components; the NSBF Interface and Disk System (NIDS), the Data Monitor (DMON) and the Data Analysis Workstation (DAW). The NIDS provides the primary interface to the NSBF operations control center ground system for uploading commands and downloading payload status information both at Palestine (NSBF OCC) and at the remote flight line (NSBF ROCC). Immediately following launch, and for about the first 24 hours of flight, ATIC control is handled from the flight line through the NSBF ROCC. During this period the LOS telemetry will allow a significant portion of the data to be downloaded and analyzed to assess instrument performance and configuration. If changes need to be made, commands can be immediately uplinked. The near real time monitoring of this data is done through the DMON and online analysis is handled by the DAW. Communication of data from the NIDS to the DAW or DMON is provided by a Remote Procedure Call (RPC) interface. While the NIDS will be a PC running the QNX operating system, RPC clients are available to a large variety of platforms. Thus, ATIC collaborating institutions can develop the DMON / DAW functionality on whatever platform they are most comfortable with.

Prior to loss of LOS, control of the ATIC payload will be handed off to the NSBF OCC where a NIDS identical to that on the flight line will be used for the remainder of the mission. In addition, both NIDS units will communicate with each other via a socket level interface over the internet link between Palestine and McMurdo. This will allow the payload to be monitored at both sites and provide a backup for operations.

3. Data Processing and Analysis

The ATIC collaboration has in place a coordinated plan for the processing and analysis of the LDB flight data. This plan is based, in part, upon the experience gained from the CERN performance validation runs and will be utilized for the flights. For an LDB, we anticipate a data volume of approximately 50 GB, which contains all housekeeping, calibration and cosmic ray event data. It must be emphasized that obtaining the 'overall' science products to be derived from ATIC -- energy spectra for individual elements -- over the largest range of energy and for the rarest elements will require the combination of results from several balloon flights. Thus, special care must be taken to insure accurate intra-flight validation of the results and to maintain each flight's dataset in a standard form for superposition with subsequent flight datasets.

E. Flight Operations

A conceptual view of the ATIC flight configuration (without NSBF equipment) is shown in Figure E.1. Participating in an LDB expedition begins in January at the Project Initiation Conference (PIC) held at Wallops Flight Facility. The payloads for the LDB campaign next undergo a complete integration/testing and Mission Readiness Review (MRR) at the NSBF

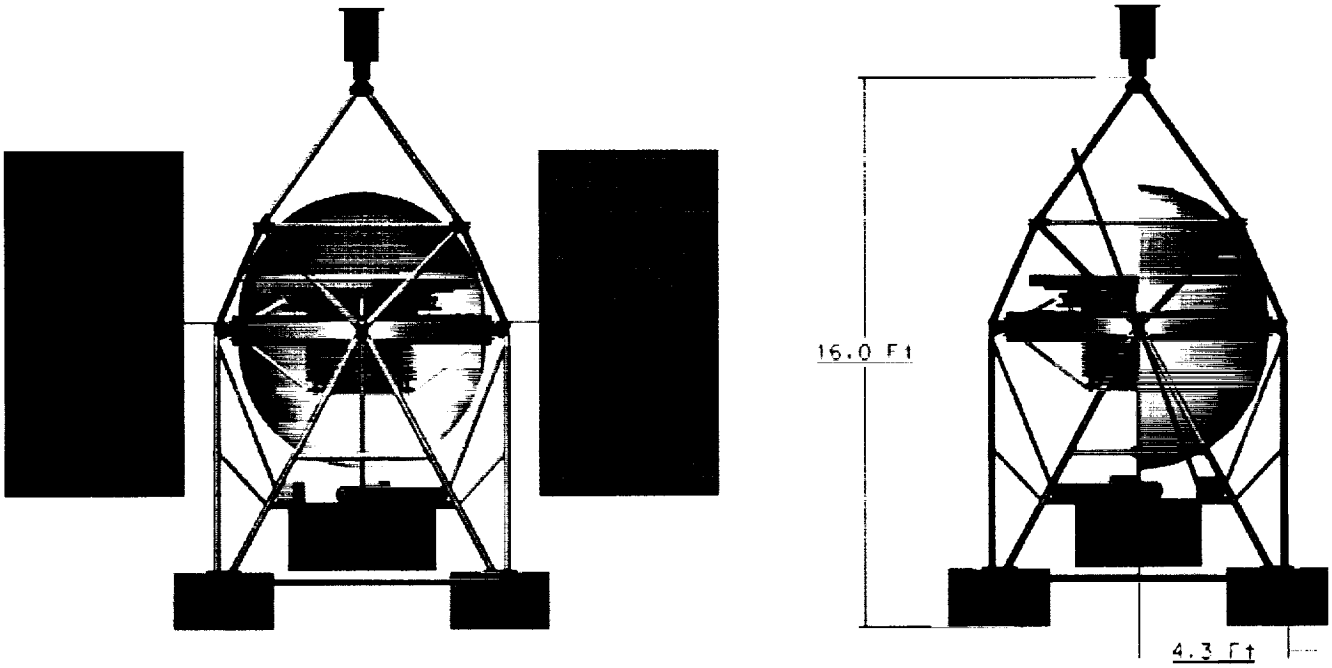

Fig E.1: The ATIC payload concept front (left) and side (right) view.

facility, Palestine, Texas in the mid-July to early August period, and are subsequently packed and shipped directly from Palestine to Port Hueneme, CA. The experiment crates are loaded onto a ship which arrives in New Zealand in October. The first science personnel arrive in late October and begin readying the experiments for flight. This past year, the 'flight ready' date was 11 December, with launches occurring in late December or early January. Recovery and re-packing must be complete by mid-February when the transport leaves Antarctica to end the season. Experiments are returned by ship to Pt. Hueneme in March.

During the pre-deployment integration at Palestine, the entire payload is assembled, and tested with the NSBF systems. For the compatibility tests, the NSBF SIP, SIP PV arrays and antennas were installed, and the total payload was operated outside with power from the PV arrays. All telemetry systems were exercised; commands into the instrument and data sent from ATIC through the transmitters. All interfaces were verified and certified for the balloon flight. Figure E.2 shows the ATIC payload at Palestine during these compatibility tests.

The first flight of ATIC, its "test" flight was flown from McMurdo, Antarctica. This became possible with the cancellation of one of the experiments selected for an LDB, and ATIC was asked to replace that experiment and perform its initial flight from McMurdo rather than from Ft. Sumner. This was an exceptional opportunity for the ATIC investigation, and the ATIC team performed superbly in meeting the accelerated schedule for the Mission Readiness Review

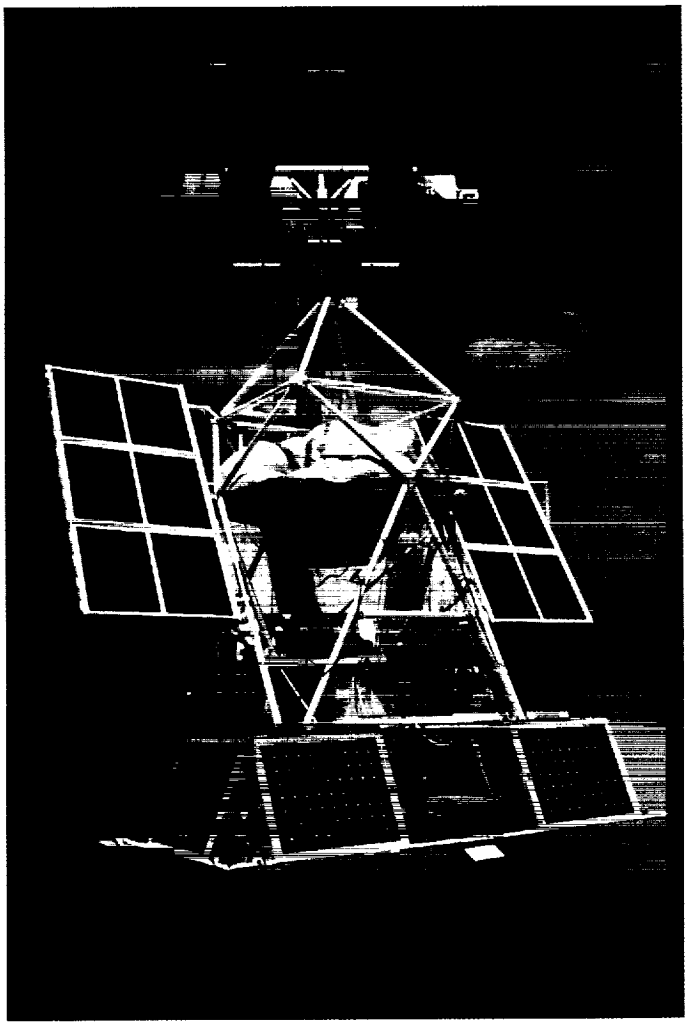

Fig. E.2: ATIC assembled and operating outside the hanger at NSBF prior to the Mission Readiness Review.

and eventually, the launch, as described below.

Prior to the LDB campaign in FY01, there was flight campaign from Lynn Lake, Canada. ISOMAX was one of the payloads, and suffered a rupture in its pressure shell during ascent. This shell, made from Kevlar, prompted a re-evaluation of the ATIC flight since ATIC also uses Kevlar pressure shells, but of a slightly different design. Moreover, an ATIC shell that had been proof tested to a pressure of 17 psi failed upon a second test at 14 psi.

The evaluation of the Kevlar shells was conducted by a team from GSFC-Wallops, following extensive consultations and material testing by the shell's manufacturers. Evaluation included inspection of a ruptured shell at LSU as well as a comparison to an undamaged shell. The Wallops team also had pictures of the ISOMAX shell to compare to the LSU shell. The analysis concluded that there was insufficient safety margin in the overall design, due to the stresses put upon the sewn seams, not the material itself. In addition, the LSU shell design was judged to be superior to the design used for ISOMAX.

Reducing the operating pressure in the shells, relieves much of the strain on the seams and brings the shell analysis well within the margins of safety usually assigned to pressure vessels. LSU proposed this solution, along with a detailed analysis, and this plan was subsequently approved by the Wallops evaluation team.

ATIC was approved to fly at <8 psi absolute internal pressure. This was judged sufficient for gondola thermal control and provided no problem of high voltage discharges. It did necessitate procuring, testing, and installing a gas relief value which could be closed and opened by command – closed on ascent as the balloon reached the appropriate pressure altitude, and opened, if necessary, during flight and after termination of the flight, prior to recovery. This system added some weight to the payload, but functioned superbly. As mentioned below, ATIC held a constant pressure throughout the flight and the Kevlar shells we recovered intact from the landing site.

The ATIC flight team arrived at the end of October and, after a week of weather related delays, began to assemble the ATIC payload in the Payload Integration Garage (PIG) at Williams Field. Other than requiring more time than anticipated, the assembly and testing of the hardware proceeded well. Figure E.3 shows some of the assembly underway at the PIG facility.

The ATIC payload was ready for flight in mid-December 2000 when the weather turned bad. There were several "roll-outs" and "roll-back-ins" before close to acceptable launch conditions were encountered. ATIC was launched on 28 December 2000 with no problems encountered. Figure E.4 shows pictures of the final flight preparations and the launch. Line-of-sight (LOS) telemetry was acquired and this allowed final adjustments to be made to the thresholds and the trigger levels, as well as assessing the instrument's health and performance. All LOS telemetry was recorded for off-line processing and analysis. The TDRSS link was also exercised, and this became the principal mode of contact for health and safety assessment, as well as commanding, once the payload left LOS telemetry range. The TDRSS data was delivered to NSBF in Palestine, TX from which it was FTP'd to the flight team in Antarctica. This link performed flawlessly. Moreover, ATIC collaborators at other institutions could access this NIDS/PIR system and download the TDRSS "snapshots" for evaluation at their home institutions. All of the flight data was recorded on-board on a 50 GB hard disk, and this is the basis for the analysis. In addition, a web site was maintained at LSU on which were placed progress reports and some of the housekeeping data from the flight. This site was made available to the public and was accessed by local school teachers as well as NASA and NSF personnel.

See http://ATIC.phys.lsu.edu/ATICweb

Figure E.5 shows the trajectory of the ATIC flight and lists the time line of events. Approximately 43.5 Gigabytes of data were recorded on-board, consisting of just over 26 million cosmic ray triggers, 1.3 million calibration records, 742,000 housekeeping records and 18,300 rate records. Over 80% of the data is useable.

As shown in Fig. E.5 the ATIC trajectory spiraled outward in latitude by a small amount, thereby missing McMurdo as a landing zone. It was necessary to allow the flight to proceed over the ROSS sea and the trans-Antarctic mountains to a point on themed-level plateau where the flight was terminated. Figure E.6 shows photographs of the landing and recovery. (Note that ATIC landed fully upright on the ice!) The ATIC components/subsystems described above can be recognized in these photographs. Although the landing site was only a few hundred miles (as the crow flies) from McMurdo, it was not accessible by heliocopter without refueling. So, recovery was via Twin Otter (see Fig. E.6, lower left) which required two trips. Due to the small size of the door in this aircraft, it was necessary to fully disassemble ATIC on-site, as shown.

Recovery was delayed due to aircraft availability and to poor flying conditions, but it was completed successfully on 25 January 01. With the exception of the parachute and main pressure vessel ring, all of the ATIC components were successfully returned to McMurdo. The remaining ATIC team members in McMurdo then re-packed the ATIC hardware into the shipping crates prior to their departure at the end of Jan./first of Feb.

The flight hard disk was recovered on the first Twin Otter recovery flight. This disk was mounted in the ATIC ground data system in the PIG facility at McMurdo, and the data was determined to be intact. The entire disk was copied, with the copy returned to the University of Maryland while the flight unit was hand carried back to LSU. Processing and preliminary analysis commenced shortly after the return of the data disks.

Figure E.3: Assembly of the ATIC Payload

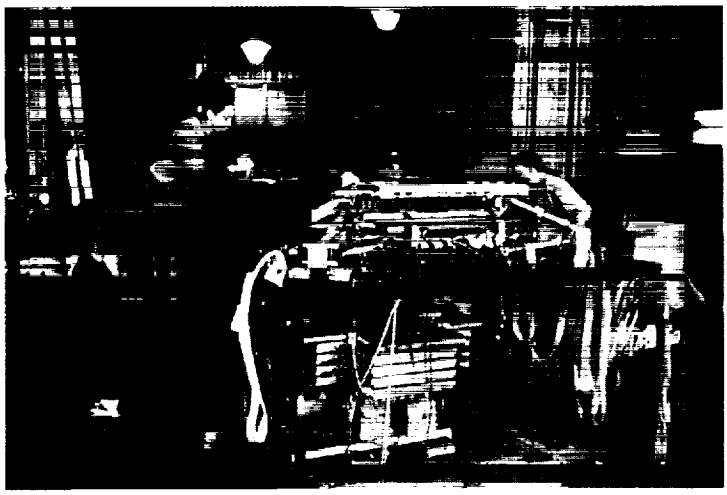

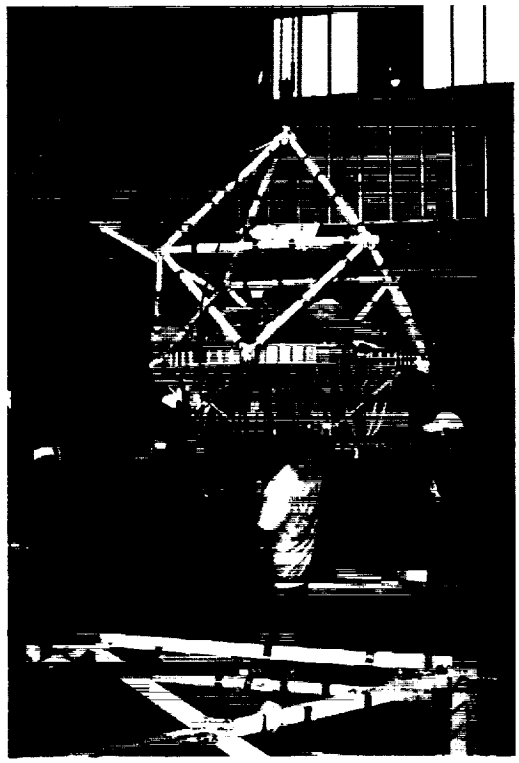

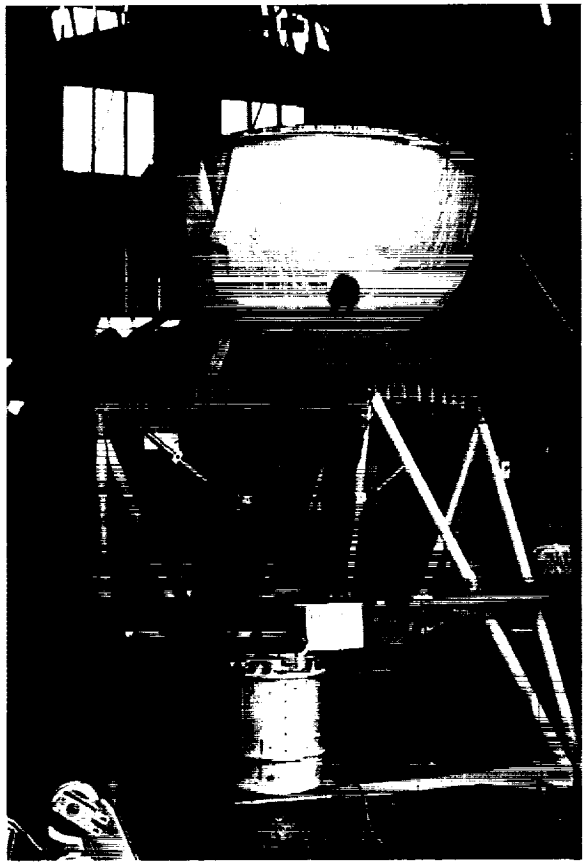

Figure E.4: ATIC is launched at 4:25 pm (local) on 12/28/00

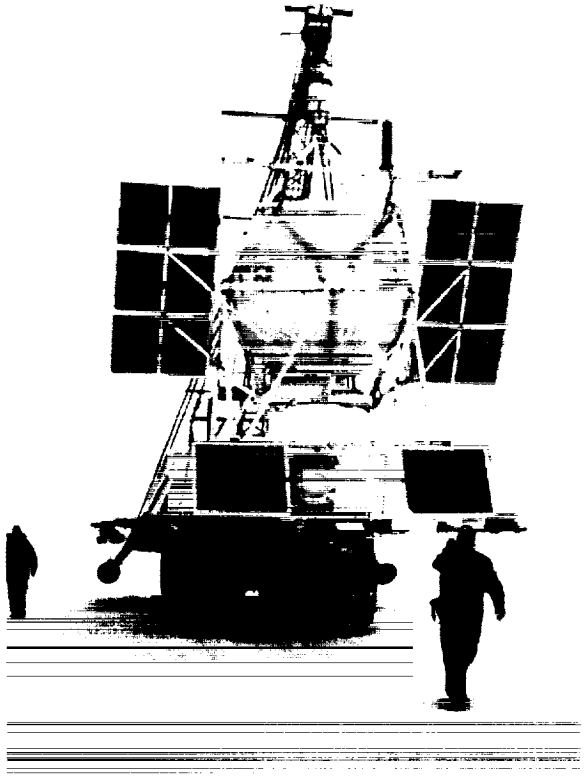

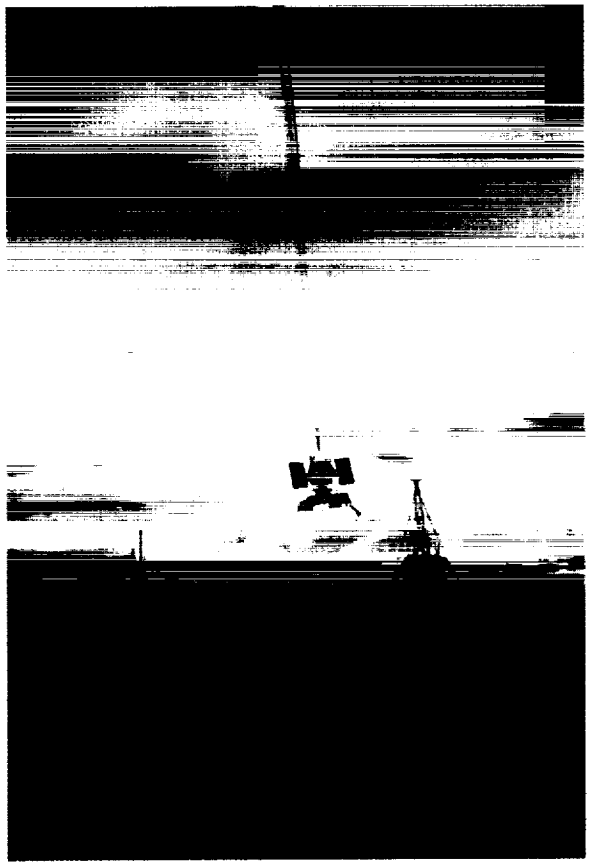

Figure E.5: ATIC Flight Trajectory

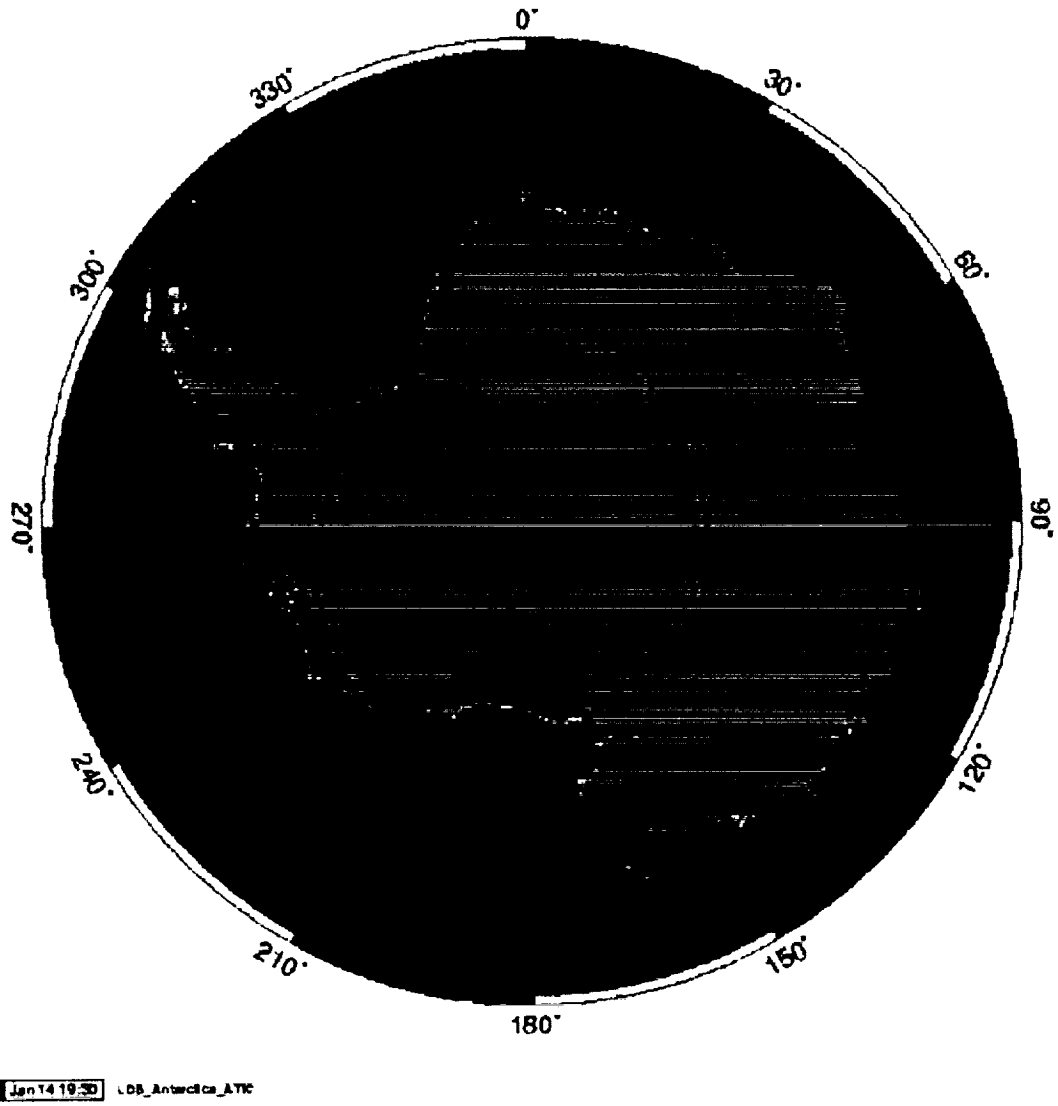

Launch:	12/28/00 04:25 UTC
Begin Science:	12/29/00 03:54 UTC
End Science:	01/12/01 20:33 UTC
Termination:	01/13/01 03:56 UTC
Recovery:	01/23/01; 01/25/01

Figure E.6: ATIC termination took place on 1/13/2001
Recovery took place on 1/23/2001 and 1/25/2001

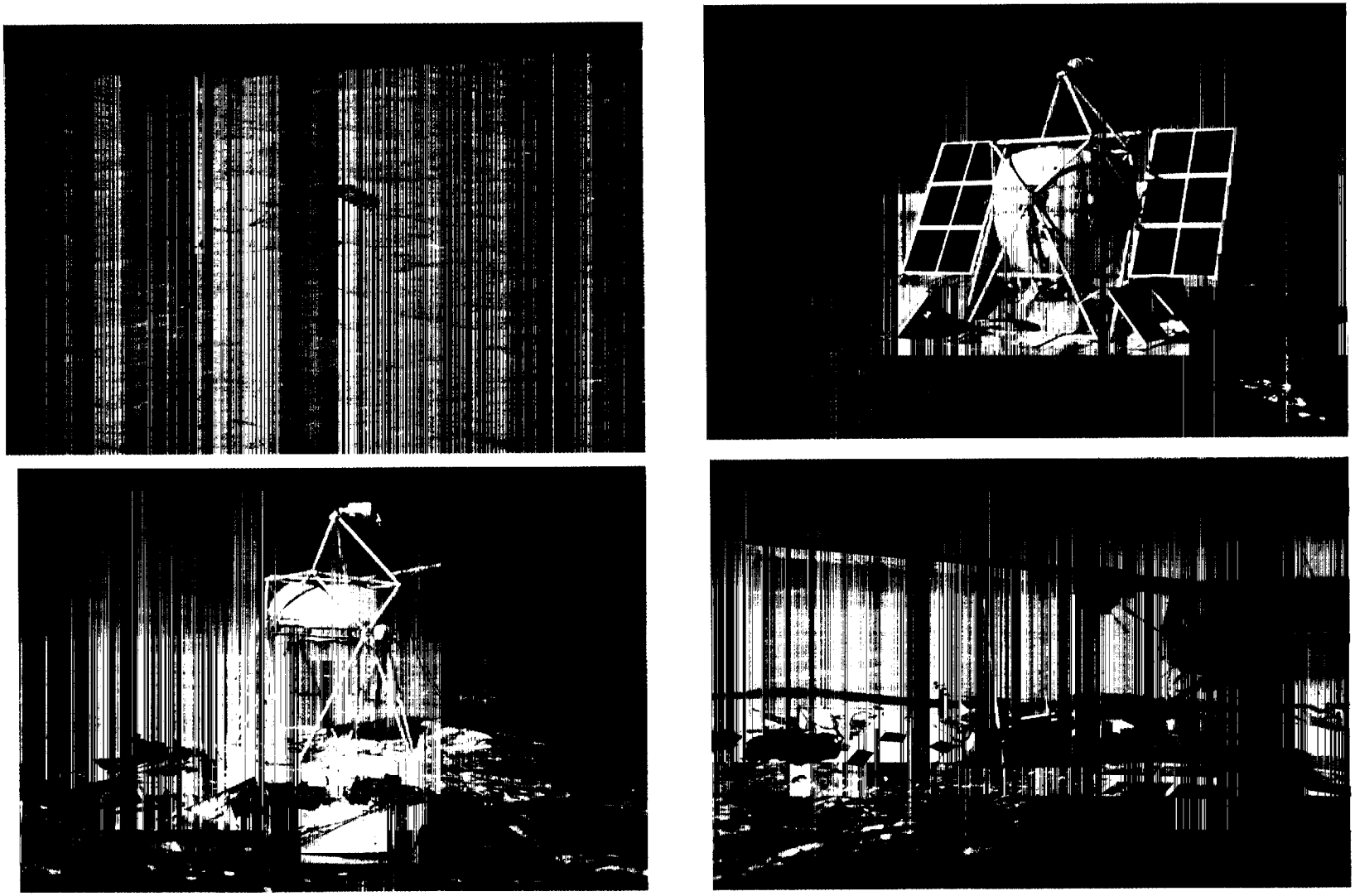

F. Preliminary Results and Performance Data

Overall, the hardware performed well. One side of S2 had an in-flight problem that has been identified and is being repaired. S1, S3 and the BGO all performed nominally, as did the Si-matrix. There were a few "noisy" channels that have been identified, and these are being fixed/replaced. Only one BGO crystal showed any appreciable physical damage (it cracked) and this one will need to be replaced. Several photomultiplier tubes broke off their light guides and these are being replaced as well.

Pre-flight there was a large concern about flying our Kevlar pressure shells around the experiment. The flight was conducted at an internal pressure of 8 psi and held constant for the entire flight with no detectable leakage. The Kevlar shells were recovered and inspected for any signs of stress.

Figure F.1 shows some of the housekeeping and performance data for the flight. The mean altitude was 37 km with a very good altitude excursion of ±1.5 km as the sun angle varied over the 24 hour day. The temperature shows similar daily fluctuations but remained within the 20-30°C range for the entire flight. The constant mean of the P/T curve demonstrates the integrity of the gondola shells.

The ATIC data has been processed to the first level using pre-launch calibrations. With 6000 channels to calibrate, the final dataset will take some time to produce -- a major task for the next year. However, even at this preliminary stage we have results on the instrument's response and performance. Figure F.2 (top) shows a cross plot of the charge measured in the scintillator hodoscopes and the Si-matrix for raw data. The H and He "islands" are readily discernable and Carbon and Oxygen are visible.

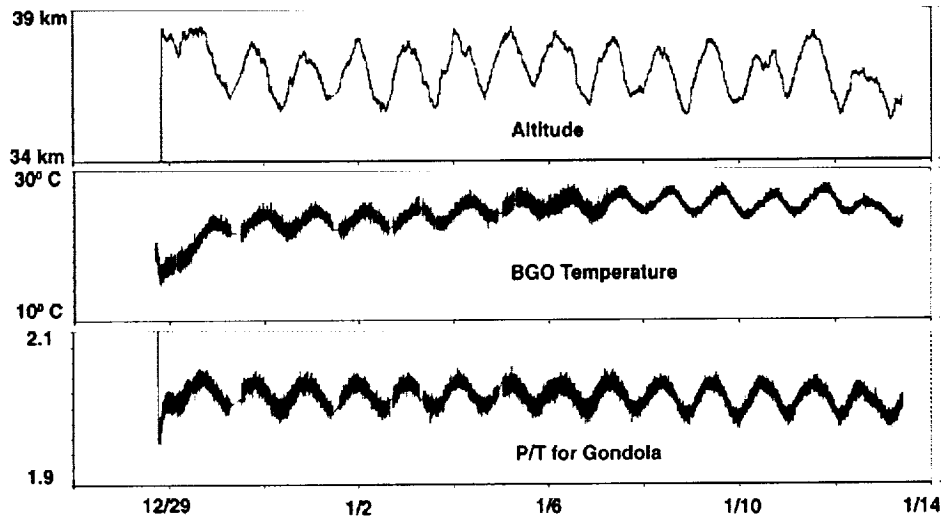

Figure F.1. ATIC payload performance during flight.

The lower part of Fig. F.2 shows the energy deposited in each layer of the calorimeter for a sample of events around 100 GeV. The shape of the curve is as expected. Note that shower maximum is occurring near the center of the calorimeter depth. Comparison of plots like this

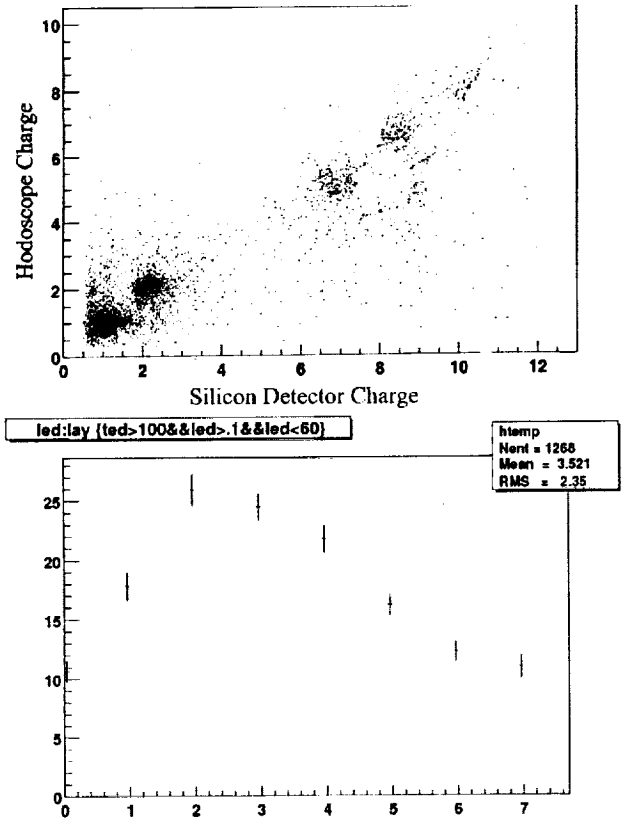

Figure F.2. Charge and Energy measurements.

with the pre-flight simulations allows us to look for channels with faulty calibrations or other problems. For the majority of the flight, we employed a low energy trigger which will allow the energy spectra to be measured down to 10's of GeV/nucleon, once the trigger efficiency as a function of energy is calibrated.

The preliminary energy deposited spectrum for a small sample of events selected to be "proton-like" in the Si-matrix and the S1 scintillator is shown in Figure F.3 with power-law spectra of different indices superposed for comparison. Power-law indices between 2.7 and 2.8 are suggested, consistent with expectations. This demonstrates that the Calorimeter and the analysis procedures are performing as anticipated, even though Fig. F.3 is still a long way from a publishable result.

As part of the on-line monitoring and analysis, the ATIC team developed an event display routine, a sample of which is shown in Figure F.4. This is a high energy event with total energy deposited in the calorimeter of ~2.8 TeV which would make it a 5-6 TeV total energy particle, probably a carbon nucleus. The size of the boxes/bars shown

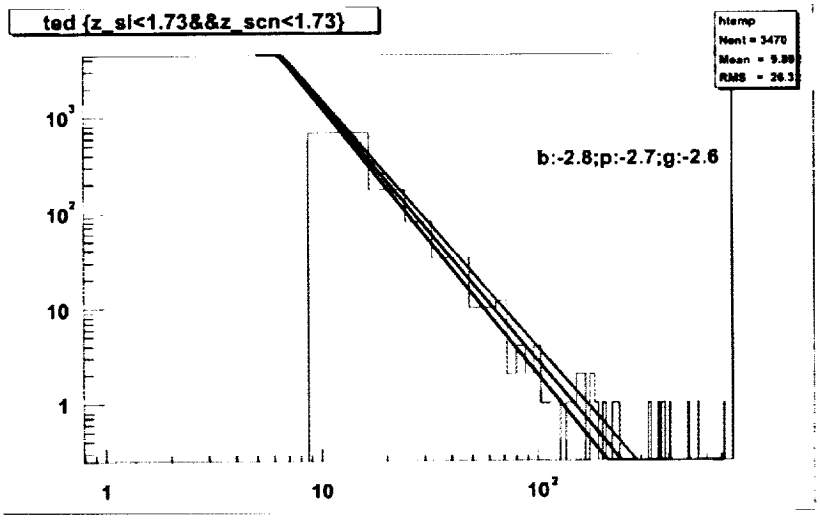

Figure F.3. Total energy deposited spectrum for "proton-like" events from the LOS telemetry with superposed power-law spectra.

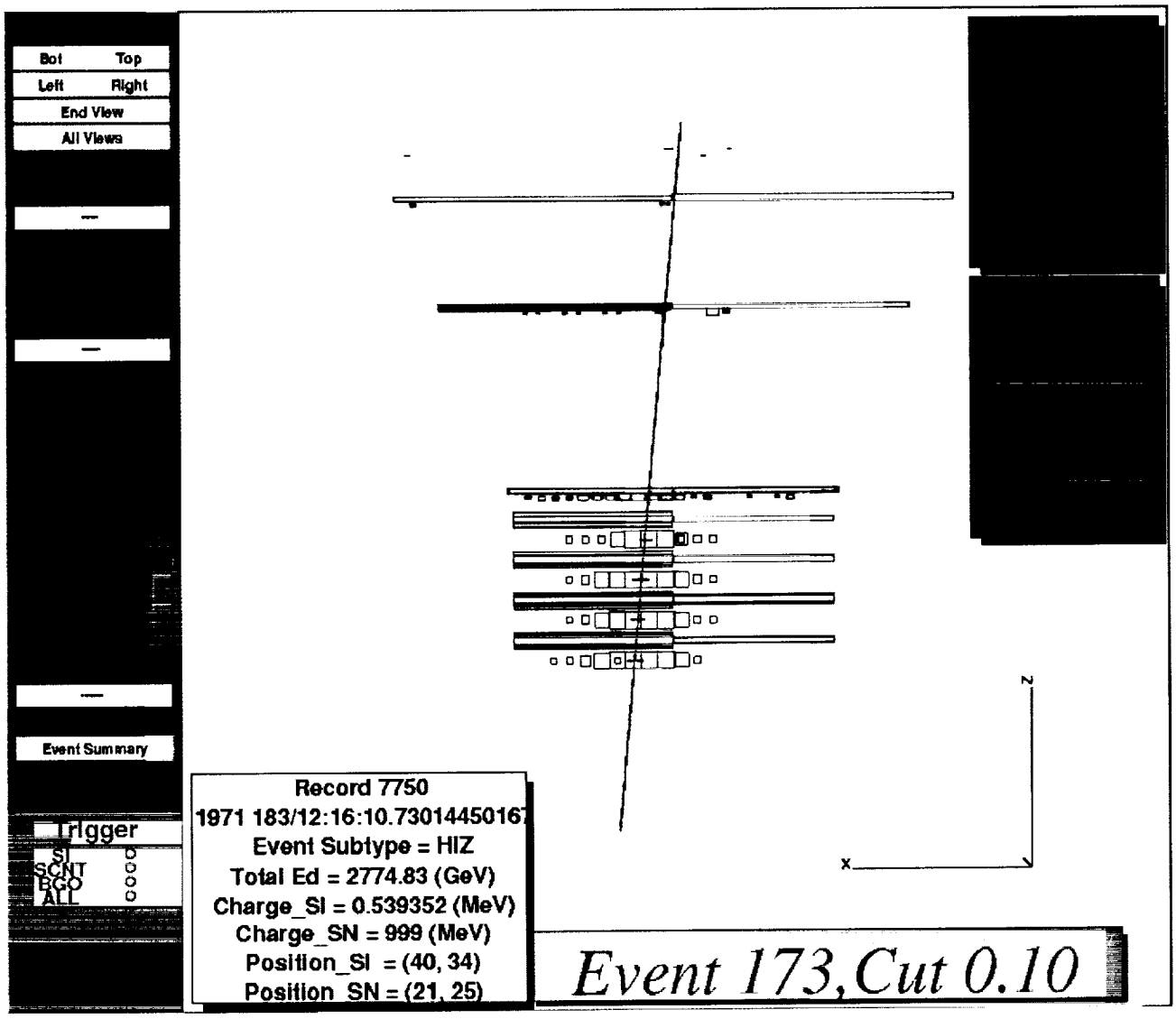

Figure F.4. Individual event reconstruction.

for each detector layer are proportional to the energy deposited in that BGO crystal, scintillator strip or Si-pixel. The particle's trajectory (shower core) is readily apparent, and the trajectory drawn delineates the line of maximum energy deposit. Note that there are multiple hits in the S2 and S3 scintillators, suggesting that the particle's initial interaction occurred between S1 and S2, and also in the Si-matrix, showing the presence of some back-scattered radiation from the cascade. The ability to visualize individual events is particularly useful in trying to understand, and de-bug, "problem" events in the data sample.

Finally, Figure F.5 shows the all-particle total energy deposited spectrum for ~70% of the total data. The events at the left of Fig. F.5 represent particles that missed, or exited the sides of, the calorimeter or did not interact before penetrating the instrument. These events will provide an in-flight calibration sample to be utilized along with the in-flight electronic calibrations to assess time or temperature dependent response corrections and to refine the absolute energy calibration, currently based on pre-flight muon events.

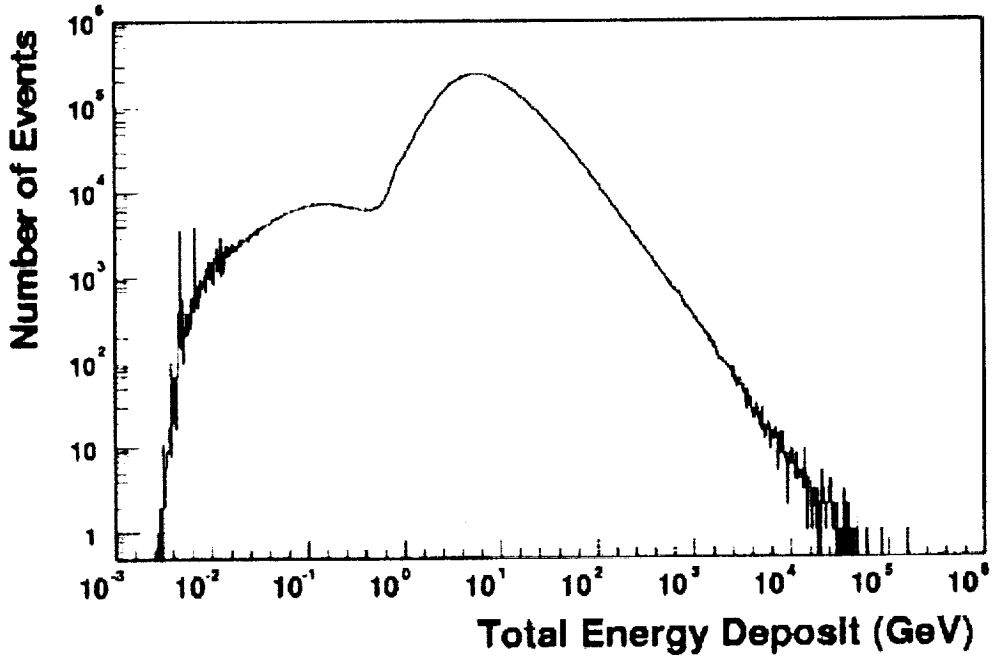

Figure F.5. All-particle spectrum in deposited energy.

During the flight data were collected in several modes ranging from S1-S3 (i.e. no BGO requirement) to S1-S3-BGO with varying thresholds on the BGO. The shape of the central region of Fig. F.5, around the peak, is determined by the different thresholds used during the flight. Initially the BGO threshold was set low in order to collect events in the 10's of GeV energy range. In order to avoid filling the flight disk, this threshold was raised (twice) as the flight extended longer than anticipated. Events in this central region must be corrected for the energy dependent trigger threshold efficiencies.

The right side of the figure shows events that were collected under all thresholds, and these must be corrected for overall efficiencies. These events follow a power law which is consistent with a differential spectrum with index of –2.7. Note that the spectrum extends to near 10^{14} eV energy deposited, i.e. events with initial total energies of 100's of TeV.

The detailed analysis of the ATIC dataset is on-going and will be completed under a subsequent grant for the ATIC project. Determining the actual spectral index, requires deconvolving the measured spectrum utilizing the resolution function and the energy dependence of the response along with all efficiency corrections. Obtaining such results is the overall goal of the ATIC analysis.

G. References

Adams, J. H., et al., the ATIC Collaboration, 1999a, "Silicon Matrix Detector for ATIC", Proc. 26th Int. Cosmic Ray Conf. (Salt Lake City), **5**, 76

Adams, J. H., et al., the ATIC Collaboration, 1999b, "The CR-1 Chip: Custom VLSI Circuitry for Cosmic Rays", Proc. 26th Int. Cosmic Ray Conf. (Salt Lake City), **5**, 69

Apanasenko, A. V., et al., the RUNJOB Collaboration, 1999, "Primary Cosmic Ray Spectra Observed by RUNJOB", Proc. 26th Int. Cosmic Ray Conf. (Salt Lake City), **3**, 163

Asakimori, K. et al., the JACEE Collaboration, 1998, "Cosmic Ray Proton and Helium Spectra -- Results from the JACEE Experiment", Ap. J., **502**, 278

Biermann, P. L., 1993, "Cosmic Rays: Origin and Acceleration, What We Can Learn From Radioastronomy", Proc. 23rd Int. Cosmic Ray Conf. (Calgary),eds. D. A. Leahy, R. B. Hicks, & D. Venkatesan, World Scientific Publ. Co., p. 45

Brun, R., et al., 1984, "GEANT Users Manual", CERN DD/EE/84-1, (Geneva) see http://asdwww.cern.ch/asd/pl/geant

Brun, R. and Radmeakers, F., 1997, "ROOT", Nucl. Instr. & Meth. **A389,** 81

Cherry, M. L., et al., the JACEE Collaboration, 1999, "Where Is the Bend in the Cosmic Ray Proton Spectrum?", Proc. 26th Int. Cosmic Ray Conf. (Salt Lake City), **3**, 187

Ellison, D. C., et al., 1994, "Supernova Remnants and the Physics of Strong Shock Waves", Publ. Astron. Soc. Pacific, **106**, 780

Ellsworth, R. W. et al., 1977, Astrophys. & Space Sci., **52**, 415

Gaisser, T. K. et al., 1995, "Opportunities in Cosmic-Ray Physics and Astrophysics", National Research Council, National Academy Press, Washington, D.C.

Ganel, O. and Seo, E. S, the ATIC Collaboration, 1998, "Improving Cosmic Ray Composition determination Through Better Tracking", Advances in Space Research, in press

Ganel, O., et al., the ATIC Collaboration, 1999, "Data Processing and Event Reconstruction for the ATIC Balloon Payload", Proc. 26th Int. Cosmic Ray Conf. (Salt Lake City), **5**, 453

Grigorov, N. L. and Tolstaya, E. D., 1999, "The Process Leading to the Formation of a 'Knee' in the Proton Spectrum at Energies of about 1 TeV", Proc. 26th Int. Cosmic Ray Conf. (Salt Lake City), **4**, 464

Guzik, T. G., et al., the ATIC Collaboration, 1996, "The Advanced Thin Ionization Calorimeter (ATIC) Experiment: Instrumentation", SPIE International Symposium on Optical Science, Engineering, and Instrumentation, Denver, CO, **2806**, 122

Guzik, T. G., et al., the ATIC Collaboration, 1999, "The Advanced Thin Ionization Calorimeter (ATIC) for Studies of High Energy Cosmic Rays", Proc. 26th Int. Cosmic Ray Conf. (Salt Lake City), **5**, 9

Kim, H. J., et al., the ATIC Collaboration, 1999, "Simulation of the ion interactions for the ATIC experiment", Proc. 26th Int. Cosmic Ray Conf. (Salt Lake City), **1**, 17

Lagage, P. O. and Cesarsky, C. J., 1983, A & A, **118**, 223.

Seo, E. S., et al., the ATIC Collaboration, 1996, "The Advanced Thin Ionization Calorimeter (ATIC) Experiment: Expected Performance", SPIE International Symposium on Optical Science, Engineering, and Instrumentation, Denver, CO, **2806**, 134

Seo, E. S., et al., the ATIC Collaboration, 1997, "Advanced Thin Ionization Calorimeter to Measure Ultrahigh Energy Cosmic Rays", Advances in Space Research, **19**, No.5, 711

Shibata, T., 1996, "Cosmic Ray Spectrum and Composition: Direct Observation", Nuovo Cimento C, **19**, 713

Waddington, C. J., et al., 1992, "GOAL", Galactic Origin and the Acceleration Limit, NASA Headquarters, Code SS, Washington, DC.

Wang, J. Z., et al., the ATIC Collaboration, 1997, "Cosmic Ray Shower Simulation and Reconstruction for the ATIC Experiment", Proc. 25th Int. Cosmic Ray Conf. (Durban), **5**, 5

Wiebel-Sooth, B. and Biermann, P. L., 1999, "Cosmic Rays", Landolt-Bornstein, Group VI, **3**, subvol. C, "Astronomy & Astrophysics - Interstellar Matter, Galaxy, Universe", p. 37, ISBN 0942-8011/3-540-56081-5, Springer Verlag Berlin/Heidelberg

Zatsepin, V. I., 1995, J. Phys. G., **21**, L31.

Zatsepin, V. I. And Sokolskaya, N. V., 1999, "Two Components in the Galactic Cosmic Rays", Proc. 26th Int. Cosmic Ray Conf. (Salt Lake City), **4**, 136